Received: 16 January 2020 | Revised: 22 April 2020 | Accepted: 5 May 2020

DOI: 10.1002/aic.16269

REACTION ENGINEERING, KINETICS AND CATALYSIS

AIChE JOURNAL

Dependence of zeolite topology on alkane diffusion inside diverse channels

Zhiqiang Liu[1] | Jian Zhou[2] | Xiaomin Tang[1,3] | Fujian Liu[4] | Jiamin Yuan[1,3] | Guangchao Li[1,3] | Ling Huang[1] | Rajamani Krishna[5] | Kuan Huang[6] | Anmin Zheng[1]

[1]State Key Laboratory of Magnetic Resonance and Atomic and Molecular Physics, National Center for Magnetic Resonance in Wuhan, Wuhan Institute of Physics and Mathematics, Innovation Academy for Precision Measurement Science and Technology, Chinese Academy of Sciences, Wuhan, China

[2]Shanghai Research Institute of Petrochemical Technology, SINOPEC, Shanghai, China

[3]University of Chinese Academy of Sciences, Beijing, China

[4]National Engineering Research Center for Chemical Fertilizer Catalyst (NERC-CFC), School of Chemical Engineering, Fuzhou University, Fuzhou, China

[5]Van't Hoff Institute for Molecular Sciences, University of Amsterdam, Amsterdam, The Netherlands

[6]Key Laboratory of Poyang Lake Environment and Resource Utilization of Ministry of Education, School of Resources Environmental and Chemical Engineering, Nanchang University, Nanchang, China

Correspondence
Kuan Huang, Key Laboratory of Poyang Lake Environment and Resource Utilization of Ministry of Education, School of Resources Environmental and Chemical Engineering, Nanchang University, Nanchnag 330031, China.
Email: huangk@ncu.edu.cn

Anmin Zheng, State Key Laboratory of Magnetic Resonance and Atomic and Molecular Physics, National Center for Magnetic Resonance in Wuhan, Wuhan Institute of Physics and Mathematics, Innovation Academy for Precision Measurement Science and Technology, Chinese Academy of Sciences, Wuhan 430071, China.
Email: zhenganm@wipm.ac.cn

Funding information
China Petrochemical Corporation, Grant/Award Number: 417012-4; Chinese Academy of Sciences, Grant/Award Number: QYZDB-SSW-SLH026; National Natural Science Foundation of China, Grant/Award Numbers: 21802164, 21902180, 21991090, 21991092, 91645112, U1832148; Natural Science Foundation of Hubei Province, Grant/Award Number: 2018CFA009

Abstract

Zeolites have been widely used for the processes of adsorption, separation, and catalysis, which are strongly correlated with molecular diffusion. However, the correlation between pore dimension and diffusion properties has not been systematically investigated so far. In this work, the diffusion properties of alkanes in six zeolites with similar pore sizes but different pore dimension have been examined. It is found that the diffusion coefficients of alkanes in zeolites are 2–5 orders of magnitude smaller than that in gas phase. Moreover, the diffusion of alkanes inside zeolites is sensitive to the pore dimension, and can be differentiated by 1-D straight, 1-D tortuous, and 3-D intersecting channels, based on the derived quantitative correlation between the diffusion behavior and pore dimension. Our work may not only provide deep insights into the effects of pore dimension on diffusion, but also benefits for the future design and practical applications of zeolite catalysts.

KEYWORDS

confined diffusion, heterogeneous catalysis, molecular simulations, zeolite catalysts

1 | INTRODUCTION

Porous materials (e.g., zeolites, MOFs and COFs) have been widely used in the fields of adsorption, separation, and catalysis,[1-4] which depends critically on the dimensional matching between adsorbate and the channels of porous materials.[5-7] Among various porous materials, zeolites, because of their porous structures with excellent activity, hydrothermal stability as well as high selectivity, have been

extensively employed in petrochemical industries for the processes of cracking, alkylation, etc.[8-11]

Up to now, more than 240 different topology structures of zeolites have been synthesized,[12] which can be divided into cage-type, 1-D channel-type, and intersecting channel-type.[13] Many applications of zeolite catalysts rely on the compatibility between the pore dimension and the molecular size of the reactants, intermediates, or products.[14,15] It is widely accepted that understanding a reaction inside the pores requires knowledge on adsorption of the reactants, diffusion of the reactants to the reaction centers, catalytic conversion of the reactants into the products, subsequently diffusion of the products away from the reaction centers, and finally desorption of the products from the zeolite.[15] It should be noted that the diffusion is essential in all these steps. Thus, comprehensive understanding of the diffusion in zeolites is necessary to reveal the mechanism of zeolite catalysis.

Recently, the importance of diffusion in the heterogeneous catalysis has been well demonstrated. Lercher et al investigated the toluene methylation in the medium pore size zeolites and found that the rates of methylation increased with respect to the diffusion of the aromatic molecules, which are slow in transportation and reaction.[16,17] It is experimentally observed that the catalyst lifetime of methanol to hydrocarbons reaction is longer in straight channels of ZSM-11 than that in tortuous channels of ZSM-5 because of the effects of diffusion paths.[18] Recently, it is indicated that the diffusion dynamics together with the reaction kinetics could significantly promote the activity of the carbonylation reaction inside MOR zeolite.[19] However, from a scientific point of view, it is quite challenging to disclose the mechanism of confined diffusion in zeolites.[20-22]

It is well known that self-diffusion coefficients (D_s) can be experimentally measured by the pulsed field gradient nuclear resonance (PFG-NMR), quasielastic neutron scattering (QENS) methods, as well as single molecule fluorescence microscopy.[23-27] Nevertheless, it is still a significant challenge to in-situ obtain D_s under the reaction conditions (e.g., high temperature and high pressure). As a powerful complement to the experimental methods, the molecular dynamics (MD) theoretical simulation provides an alternative way to obtain D_s. Previous work has demonstrated that such an advanced MD calculation can be used to investigate the influence of temperature and loading on the selectivity of specific hydrocarbons in zeolite catalysts.[15,28-30] Ghysels et al investigated the influence of composition, topology and temperature on the diffusion of ethene in several cage-type zeolites, and they introduced the concept of accessible window area to correlate the diffusion and pore size.[31] Krishna and van Baten examined the diffusion behaviors of small gas in zeolites with very different pore size (such as 3-D cage-type CHA of 3.8 Å, 1-D channel-type AFI of 7.3 Å size, 3-D intersecting channel-type MFI of 5.1–5.6 Å) and found that the diffusion coefficient is strongly dependent on the temperature and loading.[32-35] Smit et al investigated the loading dependence of methane in several zeolites with different channels, and elaborated that the diffusion difference comes from free energy profiles.[13,36,37] For zeolites possessing the similar pore, it is observed experimentally that the diffusion of reaction species possibly plays a crucial role in determining the different catalytic performance.[38,39] However, the mechanism of diffusion difference for zeolites possessing very close pore sizes is still not fully understood to date.

Alkane dehydrogenation and cracking reactions, as a typical heterogeneous catalysis, have been extensively investigated in medium pore zeolites.[40-46] In this work, by taking account of the effects of temperature, pressure, and alkanes, the combination of MD and Monte Carlo (MC) simulations have been performed to study the diffusion behavior of alkanes inside six medium pore zeolites (i.e., MFI, MEL, PON, BOF, ATO, and PSI). On the basis of the self-diffusion coefficient, diffusion trajectory, velocity autocorrelations function, and radial distribution function, the diffusion mechanism of alkanes confined inside zeolite catalysts will be elucidated. The present work may provides useful guidance for the design of zeolite catalysts with improved performance for engineering applications.

2 | MODEL AND COMPUTATIONAL DETAILS

2.1 | Zeolite frameworks

In order to systematically investigate the effect of pore structures on alkane diffusion in zeolite catalysts, some typical medium pore zeolites (i.e., MFI, MEL, PON, BOF, PSI, and ATO) with similar pore size of 5.0 ~ 5.6 Å were chosen (see Figure 1 and Table 1). It is noteworthy that only two of them (Silicalite-1 and -2, MFI, and MEL, respectively) have been synthesized, and the others in silicalite structures are hypothetical as far (they exist as aluminosilicates, gallium-aluminum germanate, and aluminophosphates). PON (Figure 1a) consists of 1-D tortuous channels (Figure 2a) with windows size of 5.0 × 5.3 Å. BOF (Figure 1b) presents a 1-D tortuous channel (Figure 2b) with a window size of 5.2 × 5.4 Å. PSI (Figure 1c) is formed by straight channels (Figure 2c) with elliptical windows of 5.0 × 5.6 Å. ATO (Figure 1d) possesses 1-D straight channels (5.4 × 5.4 Å) (Figure 2d). MFI (Figure 1e) zeolite contains 3-D intersecting channels that are derived from the straight channels (5.3 × 5.6 Å) along [010] direction (Figure 2e) intersected by zigzag channels (5.1 × 5.5 Å) running in [100] direction (Figure 2f). While MEL (Figure 1f) consists of two intersected straight channels (5.3 × 5.4 Å) respectively along [100] (Figure 2g) and [010] directions (Figure 2h).

2.2 | Computational details

MD simulations were used to investigate the diffusion behaviors of alkanes in the gas phase (homogeneous catalysis) and inside zeolites (heterogeneous catalysis). For methane (C1), ethane (C2), propane (C3) and n-butane (C4) molecules in the gas phase, NPT ensemble (constant number of particles N, pressure P, and temperature T) was used for equilibration so that the volumes were stable at various temperatures and pressures, then NVT ensemble (constant number of

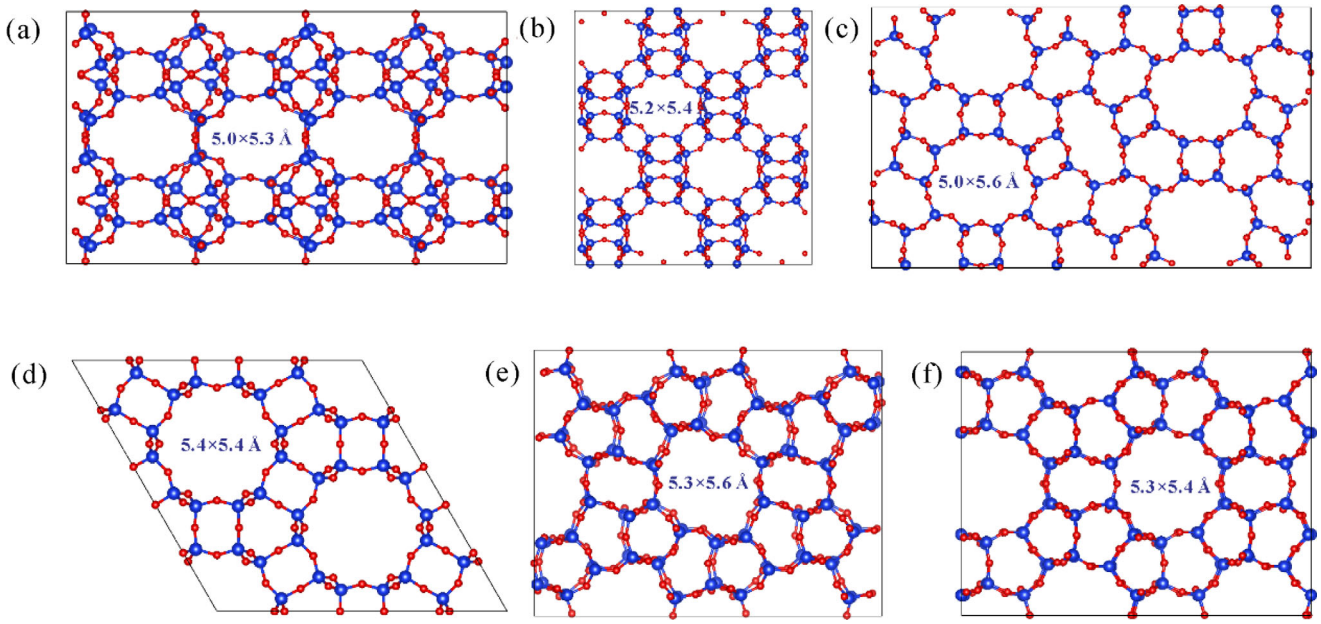

FIGURE 1 Zeolite structures with (a) PON, (b) BOF, (c) PSI, (d) ATO, (e) MFI and (f) MEL topology [Color figure can be viewed at wileyonlinelibrary.com]

TABLE 1 Channel properties of zeolites and loading number of alkanes in the MD simulation

Zeolite	Pore size (Å)	Channel type	Super cell	Volume (Å^3)	Number (pure)[a]	Number (mixtures)[b]
PON	5.0 × 5.3	Tortuous	8 × 3 × 2	62,631	24	48
BOF	5.2 × 5.4	Tortuous	8 × 2 × 2	41,423	16	32
PSI	5.0 × 5.6	Straight	10 × 2 × 1	140,823	16	32
ATO	5.4 × 5.4	Straight	2 × 2 × 16	118,973	24	48
MFI	5.1 × 5.5	Tortuous	2 × 4 × 3	126,603	24	48
	5.3 × 5.6	Straight				
MEL	5.3 × 5.4	Straight	2 × 4 × 3	129,208	24	48
	5.3 × 5.4	Straight				

[a]Loading number of alkanes at infinite dilution in each zeolite;
[b]Total loading number of molecules for the 1:1 methane/(ethane or propane or butane) mixtures.

particles N, volume V, and temperature T) was used for studying the diffusion behaviors. It is noteworthy that only NVT ensemble was used in zeolites for the change of framework volume versus the temperature can be ignored. In order to avoid the effect of thermostat on collision, NVE (constant number of particles N, volume V, and energy E) ensemble was used to study the velocity autocorrelation function (V_{acf}).

In our simulation, the initial structures of pure silicon zeolites are taken from the International Zeolites Associations (IZA) database.[12] The super cells are selected as 8 × 3 × 2, 8 × 2 × 2, 10 × 2 × 1, 2 × 2 × 16, 2 × 4 × 3, and 2 × 4 × 3 for PON, BOF, PSI, ATO, MFI, and MEL zeolites, respectively (see Table 1). The initial structures of zeolites were optimized by GULP[47] with core-shell force field[48,49] and were fixed during the subsequent MC and MD simulations. The parameters of the force field for hydrocarbon and zeolites were given in the original reference by Dubbeldam,[50] which has been widely used and could describe the adsorption and diffusion of hydrocarbon in zeolites well.[51-53] The parameters of the force field are described in the Data S1.

Grand canonical MC simulation was performed to obtain the isotherm and heat of adsorption. In the grand canonical ensemble (μVT) chemical potential, volume, and temperature are fixed. During the MC simulations four trial moves of molecules were randomly attempted: translation, rotation, reinsertion and swap with 20%, 20%, 20% and 40% probability. Each calculation was obtained by running 5×10^5 cycles after 5×10^5 cycles equilibration. To get the initial adsorption structures of alkanes inside zeolites with fixed loading, we performed MC simulation in the NVT ensemble using the Metropolis method.[54] For the purpose of comparing of the density of alkanes adsorbed in zeolites, the accessible microporous volumes were estimated using helium with the Widom's particle-insertion method.[55] For MD simulation, the simulated temperatures from 300 to 900 K (i.e., 300, 450, 600, 750 and 900 K) were considered and controlled by a Nosé-Hoover

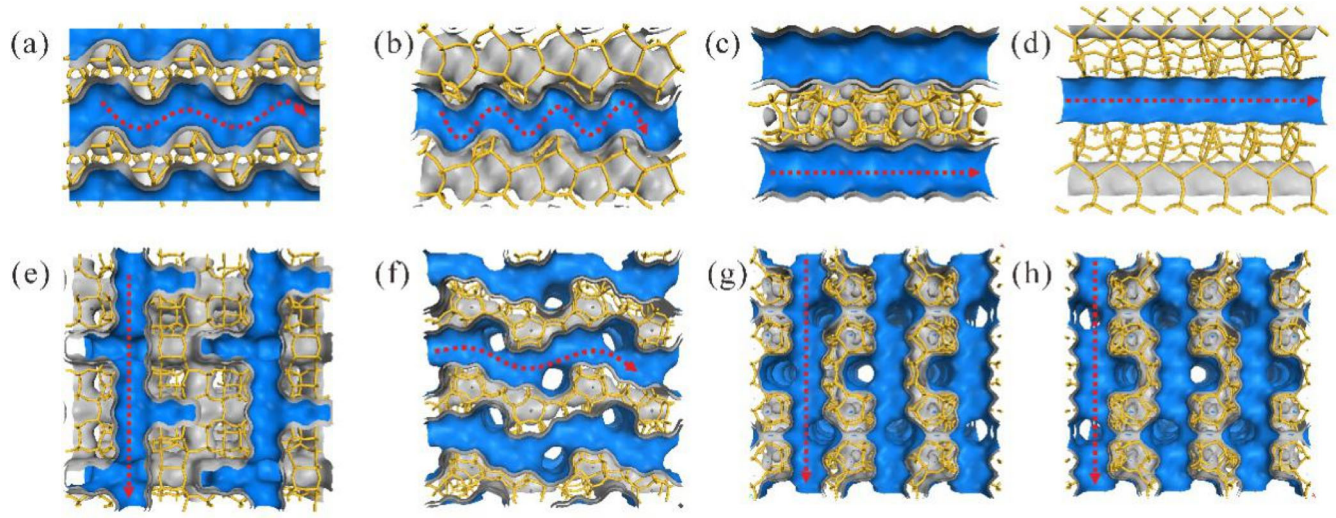

FIGURE 2 (a) 1-D tortuous channels of PON along the *x* direction. (b) 1-D tortuous channels of BOF along the *x* direction. (c) 1-D straight channels of PSI along the *x* direction. (d) 1-D straight channels of ATO along the *z* direction. 3-D MFI structure with (e) straight channels along the *y* direction and (f) zigzag channels along the *x* direction. 3-D MEL structure with straight channels along the (g) *x* direction and (h) *y* direction [Color figure can be viewed at wileyonlinelibrary.com]

thermostat[56] with a coupling time constant of 0.1 ps. The leapfrog Verlet algorithm[57] was used to integrate the Newton's equations of motion with a time step of 1 fs. Each MD simulation was equilibrated for 1×10^6 steps, then following 5×10^7 steps production for studying the diffusion behaviors of adsorbate molecules. The trajectories were recorded every 1,000 steps, while velocities were recorded every step for calculating the velocity autocorrelation function, and five independent MD simulations were carried out for better statistics. Lennard-Jones interactions were calculated with a 12 Å cutoff radius and periodic boundary conditions were also used in all three directions. MC simulations were performed by RASPA 2.0 simulation package[58] and all MD simulations were performed in the DL_POLY_2.20 code.[59]

2.3 | Diffusion coefficient

In this work, the mean square displacement (MSD) of alkanes is defined as the following equation.

$$MSD(\tau) = \frac{1}{N_m}\sum_{i}^{N_m}\frac{1}{N_\tau}\sum_{t_0}^{N_\tau}[r_i(t_0+\tau) - r_i(t_0)]^2 \quad (1)$$

where N_m is the number of gas molecules, N_τ is the number of time origins used in calculating the average, and r_i is the coordinate of the *i*-th molecule. In addition, the slope of the *MSD* as a function of time determines the self-diffusion coefficient, D_s, which is defined according to the so-called Einstein relation.[60]

$$MSD(\tau) = 2nD_s\tau + b \quad (2)$$

where *n* is the dimension of zeolites (*n* = 1 for 1-D diffusion, i.e., PON, BOF, PSI, and ATO; *n* = 3 for 3-D diffusion, i.e., MFI and MEL). The reported D_s values are calculated as the average of five independent MD trajectories.

From the diffusion coefficient (D_s) at the different temperatures, activation energy (E_a) can be obtained from the Arrhenius relationship.

$$D_S = D_0 \exp\left(\frac{-E_a}{RT}\right) \quad (3)$$

Where D_0 is the preexponential factor, *R* is the gas constant and *T* is the temperature.

3 | RESULTS AND DISCUSSION

3.1 | Adsorption characteristics of alkanes in zeolite catalysts

It is well known that adsorption and diffusion play a crucial role to determine the catalytic process inside zeolite catalysts.[15] Firstly, methane is taken as an example to discuss the adsorption characteristics of alkanes in the gas phase and inside zeolites, respectively. The density of methane under standard conditions (i.e., 1 atm and 273 K) is calculated to be 0.719 g/L in our simulation, which is in excellent agreement with the experimental value of 0.717 g/L.[61] And thus our results also further verified the validity of the force field.

Figure 3a shows that, at ambient conditions (i.e., 1 atm and 300 K), the density of methane in the gas phase turns to 0.654 g/L. As in zeolites, considering the volume of the framework, the densities

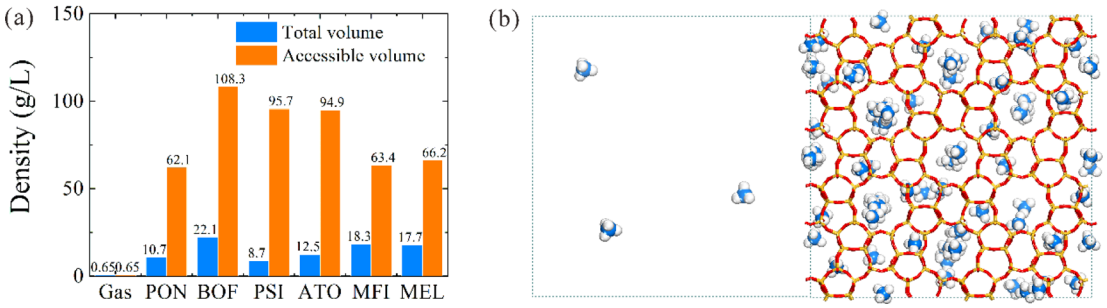

FIGURE 3 (a) Density of methane in the gas phase and inside zeolites at 1 atm and 300 K. The blue and orange bars represent the density of methane in total volume and accessible volume excluding the volume of zeolite framework. (b) Adsorption structure of methane in gas phase (left) and inside MFI zeolites (right) in the same volume at 1 atm and 300 K [Color figure can be viewed at wileyonlinelibrary.com]

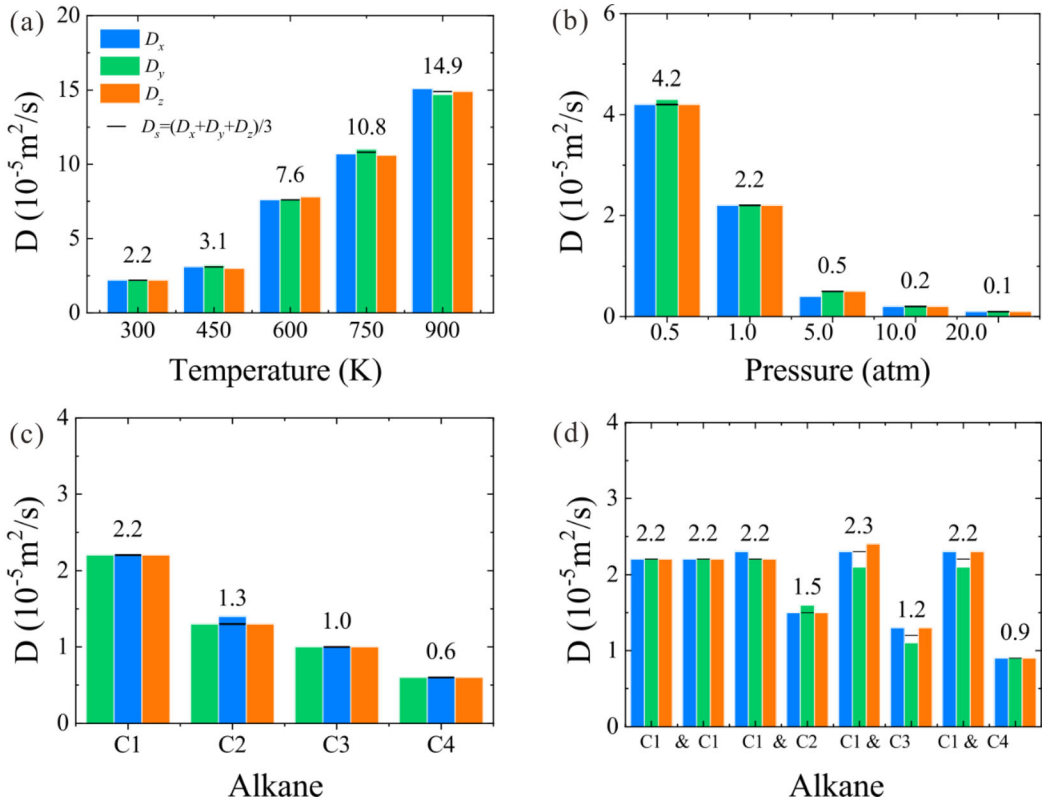

FIGURE 4 Diffusion coefficients (*d*) of alkanes in the *x* (D_x), *y* (D_y) and *z* (D_z) directions. D_s represents the average diffusion coefficients for three directions and marked by a line symbol: (a) *D* of methane at 1 atm, as a function of temperature; (b) *D* of methane at 300 K, as a function of pressure; (c) *D* of methane (C1), ethane (C2), propane (C3) and *n*-butane (C4) at ambient conditions (i.e., 1 atm and 300 K); (d) *D* of C1-C*n* mixtures (ratio of 1:1, *n* = 1–4) at ambient conditions [Color figure can be viewed at wileyonlinelibrary.com]

of methane are in the range of 8.7 to 22.1 g/L at ambient conditions, which are about 10 ~ 30 times larger than that in the gas phase with the same conditions. If only the accessible volume (the volume occupied by zeolites framework is removed) is considered, the densities of methane in zeolites are about 60 ~ 110 times larger than that in the gas phase. One adsorption structure of methane in gas phase and inside MFI zeolites are shown in Figure 3b. Furthermore, it is illustrated that the zeolites possess the ability of methane aggregation due to the strong heat of adsorption derived from the zeolite frameworks (see Data S1), the same results were observed in single-wall carbon nanohorns as well.[62] It is noteworthy that intense concentration of reactants will facilitate the participation of alkanes in the zeolite catalysis. In order to figure out the diffusion behaviors of reactants inside the confined channels, four kinds of alkanes (i.e., methane, ethane, propane and n-butane) were chosen to investigate the diffusion characteristics in zeolites catalysts.

3.2 | Diffusion characteristics of alkanes in free gas phase

Firstly, Figure 4 shows the diffusion coefficients of alkanes in free gas phase. Since the diffusion coefficients of alkanes in the gas phase are isotropic in the *x*, *y*, and *z* directions, and thus the average value D_s ($D_s = [D_x + D_y + D_z]/3$) is used to characterize the effects of temperature, pressure, chain length, and mixtures on diffusion behaviors. D_s of methane is 2.2×10^{-5} m^2/s at ambient conditions, which is in good agreement with Higgoda's work (2.3×10^{-5} m^2/s).[63] As displayed in Figure 4a, b, D_s is strongly dependent on the temperature and pressure in the gas phase. At 1 atm, D_s of methane for 600 K and 900 K are respectively 7.7×10^{-5} and 14.9×10^{-5} m^2/s, which are about 3.5 and 7 times larger than that for 300 K. Additionally, D_s are inversely proportional to the pressure at a certain temperature (see Figure 4b). For example, D_s of methane at 1 atm is 0.5 times of that at 0.5 atm, while it is 20 times faster than that at 20 atm. Such decreases of D_s might be attributed to the smaller free space inhibits the migration of methane as pressure increases. Furthermore, it is observed that D_s is sensitive to the sizes of alkanes, following the order of methane (2.2×10^{-5} m^2/s) > ethane (1.3×10^{-5} m^2/s) > propane (1.0×10^{-5} m^2/s) > n-butane (0.6×10^{-5} m^2/s) (Figure 4c).

Actually, in the process of catalysis or separation, the alkanes exist in the form of mixture, thus it is more meaningful to study their diffusion behaviors.[64] When methane is mixed with other alkane molecules, D_s of methane remains almost unchanged no matter what kind of alkanes are involved (Figure 4d). This phenomenon may be attributed to the intermolecular space large enough for methane (with small size) to move even in the mixture. While D_s of ethane (1.5×10^{-5} m^2/s), propane (1.2×10^{-5} m^2/s) and n-butane (0.9×10^{-5} m^2/s) increase slightly with respect to the case of pure components, which is due to the interaction with methane. In brief, D_s of alkanes in free gas phase is isotropic on the order of 10^{-5} m^2/s magnitude. Subsequently, the diffusion behaviors of alkanes in confined zeolites will be discussed as following.

3.3 | Diffusion characteristics of alkanes in zeolite catalysts with 1-D channels

Compared with the case of free gas phase, the diffusion behaviors in zeolite catalysts are much more complicated due to the confined pore environments, suggesting that the diffusion is strongly dependent on the dimension, shape, and structures of zeolite.[15] In the previous work, Krishna et al theoretically investigated the diffusion properties

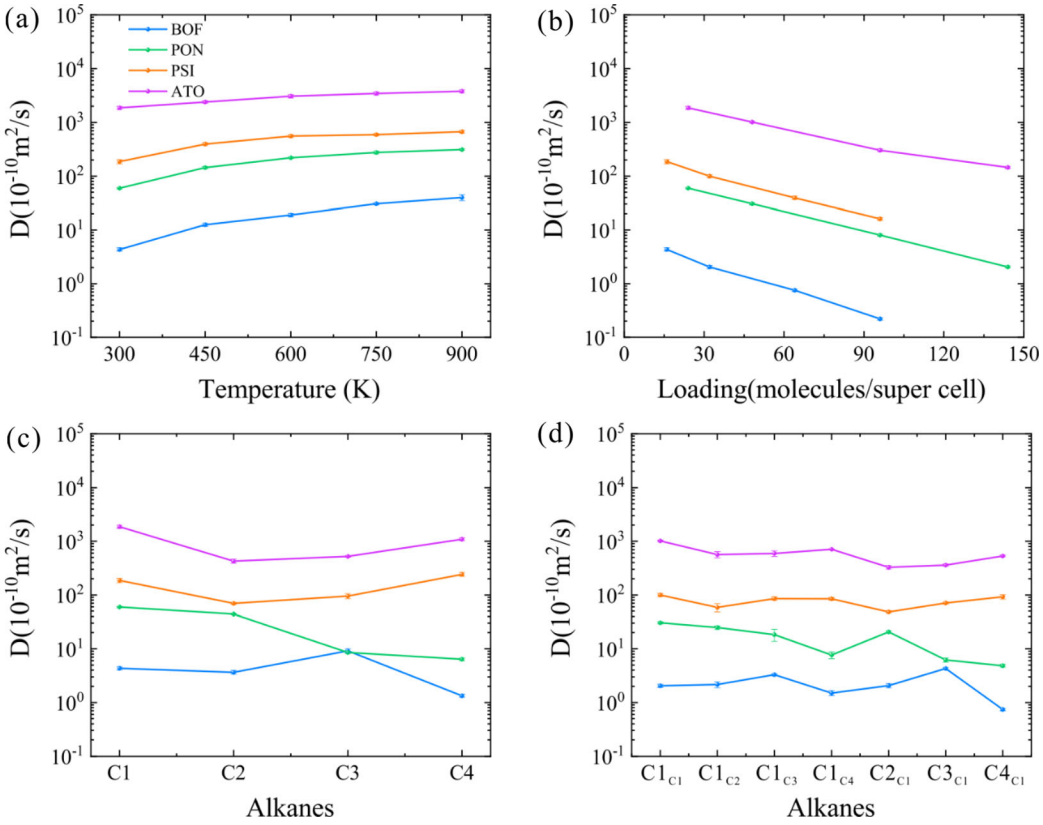

FIGURE 5 Diffusion coefficients (D_s) of alkanes inside 1-D channels of BOF, PON, PSI, and ATO zeolites: (a) D_s of methane at infinite dilution, as a function of temperature; (b) D_s of methane at 300 K, as a function of loading; (c) D_s of methane (C1), ethane (C2), propane (C3) and *n*-butane (C4) at infinite dilution and 300 K; (d) D_s of mixtures with methane and other alkane molecules at 1:1 loading and 300 K. D_s of Cx_{Cy} (*x* = 1–4, y = 1–4) represents the diffusion coefficients of C*x* when mixed with C*y* [Color figure can be viewed at wileyonlinelibrary.com]

of various gas molecules inside 8-ring, 10-ring, and 12-ring pores of zeolite catalysts. It is demonstrated that the diffusion coefficient is determined by the molecular dimensions and zeolite structures.[65] Furthermore, for zeolites with the similar 10-ring pores, it is observed experimentally that the reactant diffusion possibly plays a crucial role in inducing differences in the catalytic activity.[38,39] Therefore, it is necessary to explore the fundamental mechanism about the influence of zeolite structure with close pores on the confined diffusion behaviors.

Four 1-D zeolites with similar pores, namely BOF (5.2 × 5.4 Å), PON (5.0 × 5.3 Å), PSI (5.0 × 5.6 Å) and ATO (5.4 × 5.4 Å), were chosen as examples to investigate the diffusion properties. Figure 5 provides the diffusion coefficients (D_s) of alkanes inside 1-D channels of abovementioned zeolites. The significant difference in the molecular diffusion betweent the gas phase (10^{-5} m^2/s) and the confined pores lies in the magnitude of D_s drops 2 to 5 orders of magnitude (in the ranges of 10^{-7} to 10^{-10} m^2/s), which may be attributed to the collision between alkanes and zeolite framework. Figure 6 represents the diffusion behaviors of gas in three different 1-D channels. First, in zeolites with straight channels (e.g., PSI and ATO), D_s of methane is the fastest in the ranges of 10^{-7} to 10^{-8} m^2/s due to the minimum collision probability for methane and zeolites (see Figure 6a). While diffusion coefficients in tortuous channels with small curvature (PON) and large curvature (BOF) are respectively on the order of 10^{-9} and 10^{-10} m^2/s, which is thought to be mainly caused by the high collision probability for gas and zeolite framework (see Figure 6b and c). It should be noteworthy that such collision will result in a backward motion (green arrows), and relatively slower diffusion was observed in tortuous channel with larger curvature.

Similar with the diffusion behaviors in free gas phase, the temperature plays a crucial role in enhancing the diffusivity in the zeolite

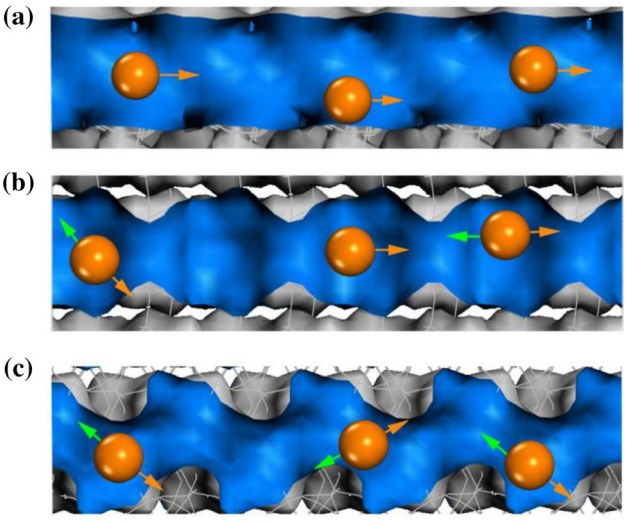

FIGURE 6 Diffusion of gas in (a) straight channels (such as PSI and ATO); (b) tortuous channels with small curvature (PON); and (c) tortuous channels with large curvature (BOF). The green arrow represents the reverse movement of gas after colliding with the zeolite framework [Color figure can be viewed at wileyonlinelibrary.com]

channels. As illustrated in Figure 5a, D_s of methane in ATO is 1.9×10^{-7}, 2.4×10^{-7}, 3.1×10^{-7}, 3.5×10^{-7} and 3.8×10^{-7} m^2/s at 300, 450, 600, 750 and 900 K, respectively, suggesting that D_s increases with the temperature rising. Comparing with D_s raised in the gas phase mentioned above, the less sensitivity of D_s in zeolites with the increasing of temperature means that confinement of zeolites will slow down the upward trend, this might be the result of higher frequent collisions between methane and zeolite framework at high temperature. Similar results are also found in PSI with straight channels, that are D_s of methane are 1.9×10^{-8}, 4.0×10^{-8}, 5.6×10^{-8}, 5.9×10^{-8} and 6.7×10^{-8} m^2/s at 300, 450, 600, 750, and 900 K, respectively. As to D_s at 300 K in PON, it increases to four times at 600 K and five times at 900 K. However, the effect of temperature is more obvious in BOF, where D_s increases to five times at 600 K and 10 times at 900 K. This may because the effect of temperature on the increase of D_s in PON is not dominant due to the low diffusion barrier, while for tortuous channel with larger curvature (BOF), the diffusion barrier of methane seems much easier to overcome with sufficient kinetic energy derived from the higher temperature. Thus, D_s is much more sensitive to temperature in tortuous channels with larger curvature. In addition, there is an excellent linear relation between ln (D_s) and 1,000/T with the temperature range from 300 to 900 K in these four 1-D zeolites (Figure 7a). The activation energies in BOF (8.2 kcal/mol) and PON (6.3 kcal/mol) with tortuous channel are higher than those in PSI (4.8 kcal/mol) and ATO (2.7 kcal/mol) with straight channels.

Diffusion behaviors in zeolites will also be affected by the loading number of adsorbents.[13,36] Figure 5b shows D_s of methane is a function of loading at 300 K. Taking ATO zeolite as an example, it is found that D_s of methane decreases as the loading increases. D_s with 24 methane (1.9×10^{-7} m^2/s) is larger than that with 48 methane per super cell (1.0×10^{-7} m^2/s), while it is 13 times higher than that with 144 methane (0.14×10^{-7} m^2/s), which implies that the loading number will also affect the diffusion behaviors in zeolites, but it is not the same as the inversely proportional decrease in the gas phase. The same tendency is also found in other zeolites (i.e., BOF, PSI, and PON). This is supported by Smit's analysis on the diffusivity, which is a decreasing function of loading due to the higher free energy.[13]

As for different alkanes, Figure 5c shows that, D_s decreases as the size of the alkane increases. For example, D_s are monotonically decreasing for methane (5.9×10^{-9} m^2/s), ethane (4.4×10^{-9} m^2/s), propane (0.86×10^{-9} m^2/s) and n-butane (0.64×10^{-9} m^2/s) in PON zeolite. However, it is noteworthy that this trend is not rigorously followed by BOF, D_s of propane is 9.2×10^{-10} m^2/s, which is larger than that of ethane (3.7×10^{-10} m^2/s) and methane (4.3×10^{-10} m^2/s). The main reason for this unusual phenomenon is probably attributed to the resonant diffusion, which shows an interesting periodic function of chain-length dependence for diffusion in zeolites. Generally, the resonant diffusion only occurs when the end-to-end chain length of a molecule matches the periodic zeolites lattice, meanwhile, the molecules synchronously occupy both low- and high-energy areas of channels, hence would experience a relatively lower diffusion barrier.[66] A famous resonant diffusion phenomenon in LTL and MTW

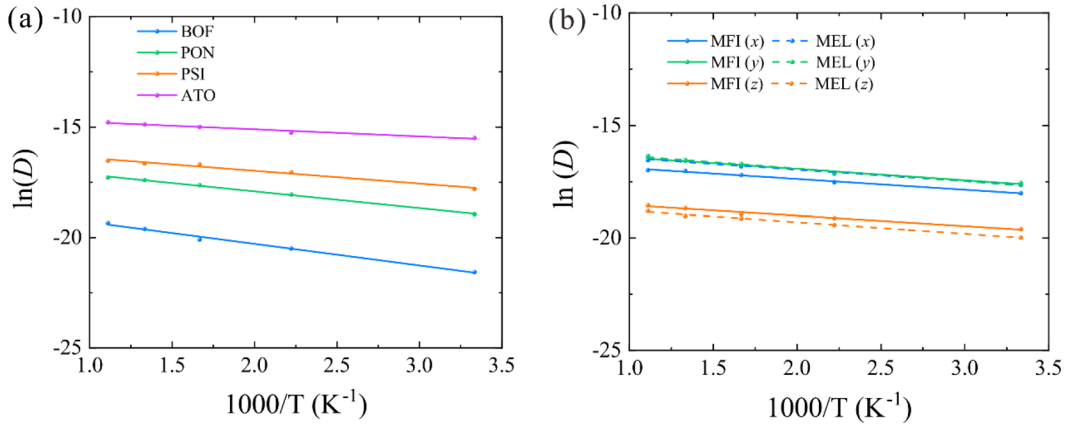

FIGURE 7 Arrhenius plots of diffusion coefficients (D_s) of alkanes as a function of temperature at infinite dilution inside (a) 1-D channels of BOF, PON, PSI and ATO zeolites; (b) 3-D channels of MFI and MEL zeolites in the *x*, *y*, and *z* directions [Color figure can be viewed at wileyonlinelibrary.com]

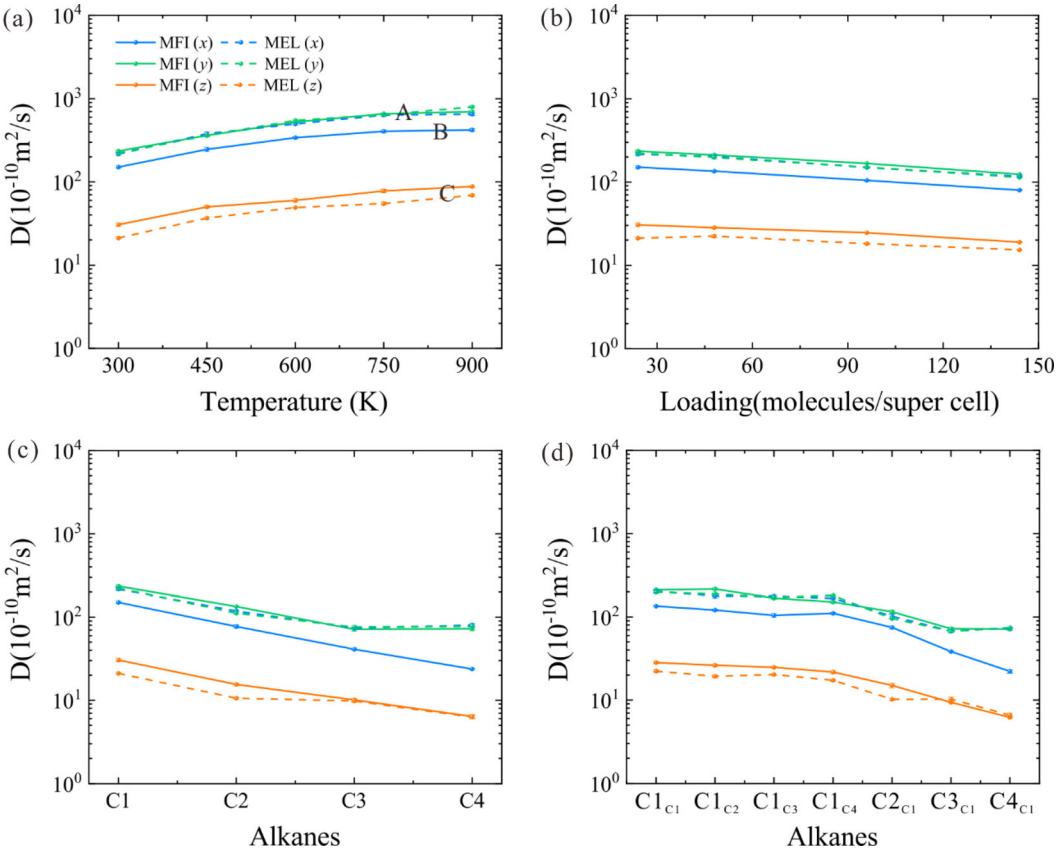

FIGURE 8 Diffusion coefficients (D_s) of alkanes inside MFI and MEL zeolites in the *x* (red), *y* (green), and *z* (blue) directions: (a) D_s of methane at infinite dilution, as a function of temperature; (b) D_s of methane at 300 K, as a function of loading; (c) D_s of methane (C1), ethane (C2), propane (C3) and *n*-butane (C4) at infinite dilution and 300 K; (d) D_s of mixtures with 24 methane and 24 other alkane molecules at 300 K. The solid and dotted lines represent D_s inside MFI and MEL. A, B, and C respectively represent D_s along straight channels, along zigzag channels, and in the z direction. D_s of Cx_{Cy} (x = 1–4, y = 1–4) represents the diffusion coefficient of C*x* when mixed with C*y* [Color figure can be viewed at wileyonlinelibrary.com]

zeolites has been reported experimentally.[67] Actually, such resonant diffusion also occurs in the mixed systems. As shown in Figure 5d, in BOF zeolite, D_s of propane (4.3×10^{-10} m^2/s) is relatively faster than methane (2.0×10^{-10} m^2/s) in the methane-propane mixtures. Except resonant diffusion, alkane presents a similar diffusion behavior with that in pure component. For example, D_s of alkanes inside PON follows the order: methane ($C1_{C1}$) > ethane ($C2_{C1}$) > propane ($C3_{C1}$) > n-butane ($C4_{C1}$) when they mixed with methane, which is the same

as that in pure component (C1 > C2 > C3 > C4). Briefly, the diffusion coefficients of alkane molecules in 1-D zeolites are in the range of 10^{-7} to 10^{-10} m^2/s, which will be strongly affected by temperature, loading, as well as dimension of alkanes and zeolites.

It is well known that the composition (e.g., aluminum) of zeolites will also affect the diffusion of gas molecules. Ghysels et al investigated the impact of chemical effects on olefins diffusion; they found that the diffusion coefficient of ethene would be decreased when the zeolite frameworks contain Brønsted acid sites. [31] Ban et al found that the diffusion of alkanes would be slowed down as Si/Al decreased for MOR zeolite. [68] Therefore, the zeolite component and Brønsted acid sites will affect the alkane diffusion to some extent. It is noteworthy that this work mainly focuses on the influence of topological structure (i.e., pure Si framework) on the diffusion, and the effect of zeolite component (e.g., aluminosilicates, aluminophosphates and so on) will be discussed in the further work.

3.4 | Diffusion characteristics of alkanes inside zeolite catalysts with 3-D channels

To the best of our knowledge, the diffusion behaviors in zeolites with 3-D channels are more complicated due to their anisotropy.[15,36] Since MFI and MEL zeolites possess the typically 3-D intersecting channels, they have been extensively used as solid acid catalysts in heterogeneous catalysis, such as alkane dehydrogenation and crack reactions.[42-45] For MFI zeolite (Figure 2e, f), it contains 10-ring straight channels along the *y* direction, intersected by 10-ring zigzag channels along the *x* directions. While MEL (Figure 2g, h) consists of two intersected 10-ring straight channels. Figure 8 describes the self-diffusion coefficients (D_s) of alkanes along three directions in MFI and MEL zeolites. However, it is found that there is similarity between the diffusion behavior in 3-D and 1-D channels, namely diffusion coefficients of methane in MFI and MEL increase with temperature rising while decreasing due to the raised loading, some significant difference still lies between the case of 3-D and 1-D channels.

In contrast to the isotropic diffusion in the gas phase or the single directional diffusion in 1-D channels, the anisotropic diffusion in 3-D channels is present for MFI and MEL zeolite (see Figure 8). Anisotropic diffusion has also been observed in experiment, for example, Hong et al have found that the diffusion coefficient of methane in the *z* direction is slower than that in the *xy* plane inside MFI zeolite by methods of pulse field gradient NMR.[69] Interestingly, it is found that the diffusion behaviors in MFI and MEL can be divided into three types (see Figure 8a): the first one is in the straight channels marked as A, including the diffusion along the *y* direction (D_y) of MFI, as well as along the *x* and *y* direction of MEL; the second one is in the zigzag channels marked as B, including the diffusion in the *x* direction (D_x) of MFI; the third one is the diffusion along *z* direction (D_z) of MFI and MEL marked as C. Figure 8a shows that the diffusion coefficients for methane adsorbed inside the straight channels (A) and zigzag channels (B) of MFI are 2.35×10^{-8} m^2/s and 1.51×10^{-8} m^2/s at 300 K, respectively. Apparently, D_s in the straight channels (D_y) is ca. 1.6 times larger than that inside zigzag channels (D_x), which is in line with Smit's description on the ratio of D_y/D_x which equals to 2 in MFI.[36] Apart from this, it is observed that the diffusion along the *z* direction is the slowest (on the order of 10^{-9} m^2/s), mainly because there is no throughout channels along this direction and the alkane can only move inside and outside the intersecting pore between the straight and zigzag channels. And this kind of anisotropic diffusion has also been observed for the movement of alkanes inside MEL zeolites. It is noteworthy that, such anisotropy of diffusion inside zeolites can be used in separation and heterogeneous catalysis. For example, since the diffusion barrier difference between *p*-xylene and *o*-xylene in nanosheet MFI (along *y* direction) is higher than that in the bulk MFI, the enhanced diffusion performance only in the *y* direction could promote the xylene separation process.[70] In addition, the activation energies are also derived from the relation between ln (D_s) and 1,000/T for methane inside MFI and MEL as illustrated in Figure 7b, and it is observed that activation energies are very similar (about 4 kJ/mol) along three directions which may due to the good connectivity in both MFI and MEL. However, significant differences in the preexponential factors (D_0) are present along three directions (see Figure 7b). D_0 of methane are 7.4×10^{-8}, 1.2×10^{-7} and 1.4×10^{-8} m^2/s in MFI, while they are 1.2×10^{-7}, 1.4×10^{-7}, 1.2×10^{-8} m^2/s in MEL along the *x*, *y*, and *z* directions, respectively. Overall, methane prefers to diffuse along the straight channel of MFI and MEL at various temperatures.

As to the effects of loading number, chain lengths and mixtures of alkanes have been shown in Figure 8b-d, for both MFI and MEL, it is found that as the loading number increases, D_s decreases in all three directions; in addition, it is illustrated that D_s of alkanes decrease with the chain lengths increase. Interestingly, it seems that longer alkane prefers to diffuse through the straight channel, as D_s of n-butane in zigzag channel is 3.0 times larger than that in straight channels, while for methane it is 1.6 times at the same condition. In the case of mixture, it should be noted that the diffusion of the components related through the thermodynamic factor (a function of the derivative of the activity coefficient against the molar fraction) is necessary. The Maxwell-Stefan (M-S) formulation for mixture diffusion is particularly convenient because it allows the estimation of diffusivities in mixtures using input data for the constituent unary components[30,71,72] . In this work, the M-S model was used to estimate the self-diffusion coefficient in binary mixtures; the calculation details are provided in the Data S1. It is found that the estimation of self-diffusion coefficients for mixture diffusion from unary self-diffusion coefficients and unary M-S diffusion coefficient are in good agreement with the values determined from MD simulations for binary mixture diffusion (see Table 2). For example, the self-diffusion coefficients of C1 and C3 extracted from mixture in MFI predicted by Maxwell-Stefan model was 105.1×10^{-10} and 46.9×10^{-10} m^2/s, which were close to values calculated by MD simulation (C1: 99.2×10^{-10} m^2/s; C3: 40.1×10^{-10} m^2/s). As shown in Table 2, although the diffusion of methane is always faster than other bulky alkanes, D_s of methane is slowed down in all three directions due to the hindrance of other alkanes. Therefore, in 3-D intersecting channels, there is an anisotropy

TABLE 2 Self-diffusion coefficients ($D \times 10^{-10}$ m^2/s) of mixtures inside MFI and MEL zeolites in three directions with 48 molecules (24 methane (C1) and 24 methane (C1)/ethane(C2)/propane(C3)/n-butane (C4)) at 300 K[a]

Mixture	Alkane	MFI					MEL				
		D_x	D_y	D_z	D_s	D_{MS}	D_x	D_y	D_z	D_s	D_{MS}
C1–C1	C1	135.0	210.8	28.3	124.7	124.7	202.7	197.5	22.3	140.8	140.8
C1–C2	C1	120.9	215.5	26.2	120.9	112.0	178.3	188.9	19.3	128.8	128.7
	C2	74.8	115.2	15.0	68.3	77.7	101.6	95.8	10.2	69.2	77.8
C1–C3	C1	104.5	168.4	24.8	99.2	105.1	177.2	170.4	20.3	122.6	121.6
	C3	38.5	72.3	9.4	40.1	46.9	67.8	67.4	10.3	48.5	59.8
C1–C4	C1	110.8	151.1	21.8	94.6	102.3	167.5	180.5	17.3	121.8	121.3
	C4	22.2	71.5	6.2	33.3	36.6	73.3	74.6	6.6	51.5	57.0

[a]D_x, D_y, and D_z represent self-diffusion coefficients along the x, y, and z directions. D_s and D_{MS} represent total self-diffusion coefficients calculated by MD simulation and estimated by Maxwell-Stefan model, respectively.

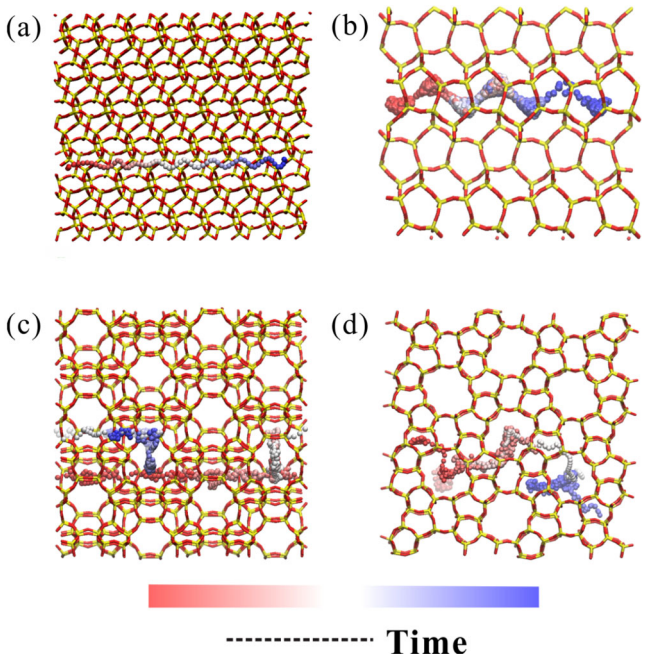

FIGURE 9 Trajectory of one methane inside (a) ATO in [100] direction; (b) BOF in [001] direction; (c) MFI in [100] direction; and (d) MFI in [010] direction. The trajectories are colored with time proceeding (red→white→blue) [Color figure can be viewed at wileyonlinelibrary.com]

and the diffusion is strongly dependent on each interconnected 1-D channels.

3.5 | Insight into the mechanism of confined diffusion

In order to get a deep insight into the mechanism of confined diffusion in zeolite catalysts, by taking methane as an example, the diffusion trajectory, velocity autocorrelation function (V_{acf}) and radial distribution function (RDF) will be further discussed. Since the trajectory obtained from MD can trace the diffusion process of molecules in microscopic view.[73,74] Therefore, the trajectories of methane moving inside microporous 1-D straight ATO and PSI, 1-D tortuous BOF and PON, 3-D intersecting MFI and MEL zeolites have been studied to clarify the diffusion process.

Figure 9 shows the diffusion process of one methane inside microporous zeolites by using MD simulations. In straight channels of ATO, due to the confinement of zeolite framework, methane can only move along 1-D main channels (see Figure 9a). It should be pointed out that methane moves along one direction with less probability of reverse movement due to the less collision. While in tortuous channels of BOF zeolite, it shows that methane stays in the same region with overlapped trajectory (see trajectory in Figure 9b, red→white→red→blue→red→blue) due to repeatedly collides with the zeolite, which slow down the diffusion behaviors. In 3-D MFI zeolite with intersecting channels, methane shows anisotropic diffusion which can move in straight channels along the y direction (Figure 9c) and in zigzag channels along the x direction (Figure 9d). The diffusion behaviors of methane in PON, PSI, and MEL are similar as that inside ATO, BOF, and MFI zeolites, respectively.

Besides the trajectory, velocity autocorrelation function (V_{acf}) is also a powerful tool to describe the diffusion and collision behavior inside zeolite and other confined systems[60,75,76] On the basis of V_{acf}, the correlation between diffusion and collision can be derived. Generally, the shorter the relaxation time of the velocity, the more frequent collisions and the slower the diffusion are. On the other hand, the larger the positive region of V_{acf}, the faster the diffusion is, and vice versa. Mitra et al investigated the motion of propene in ZSM-5 and Na-Y zeolites, suggesting that a negative region of V_{acf} come from the molecule suffers a collision with zeolite channels.[77] Figure 10a depicts V_{acf} of methane in zeolites and gas phase, respectively, where the negative value of V_{acf} represents methane colliding with other molecules and then moving in the opposite direction. It is observed that the time scale for V_{acf} in the gas phase (1 ns) is about three orders of magnitude larger than that in zeolites (1 ps), thus the diffusion coefficient in gas phase is much larger than that in zeolites. Negative V_{acf} appears the fastest in the tortuous channels of PON and BOF zeolites,

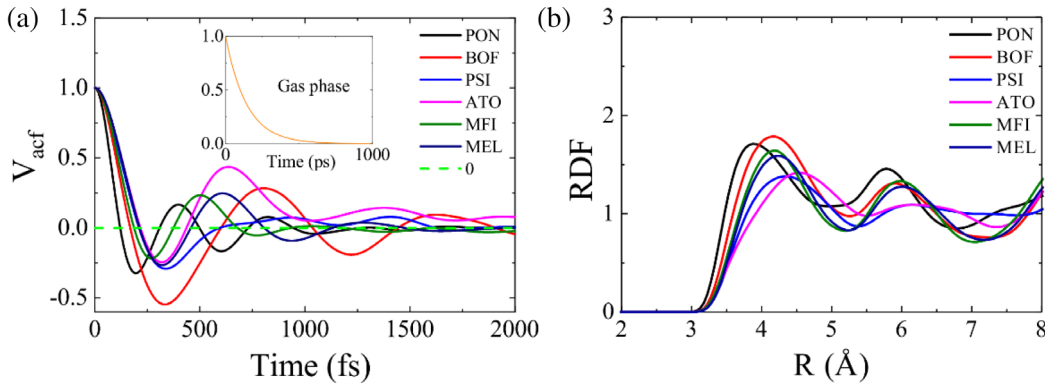

FIGURE 10 (a) The velocity autocorrelation function (V_{acf}) in zeolites or gas phase (Insets) at 300 K. (b) Radial distribution function (RDF) of methane (C atom) and zeolites (O atom) at 300 K. The loading numbers are shown in Table 1 [Color figure can be viewed at wileyonlinelibrary.com]

which shows methane is easy to collide with the zeolite framework and then moves with velocity in the opposite direction. Furthermore, it should be noted that in BOF zeolites, V_{acf} possesses the largest negative peak value, which means the probability for backward movement with fast velocity after collision in BOF is the highest, thus resulting in the slowest diffusion. While the relatively longer time for negative V_{acf} seems to be close in MFI, MEL, PSI, and ATO zeolites, suggesting that methane owns the less collision probability in these channels. The diffusion of methane in ATO zeolite is the fastest, that is because the time for V_{acf} reduced to zero is the longest, and the value of the first negative peak appeared is the smallest, which means the gas owns the least collision probability within framework.

In addition, the RDF can be employed to reflect the density varies as a function of distance from a reference particle (atoms, molecules, colloids, etc.), and the larger peaks with smaller distance indicate their more proximity.[60,76,78] For zeolites with 1-D tortuous channels, as displayed in Figure 10b, the dominant peaks for PON and BOF shows the largest values of RDF (1.71 and 1.79) and the shortest distance of C (methane)-O (zeolite) (3.9 and 4.2 Å), which indicates the strongest confinement. In 1-D straight channels of PSI and ATO zeolites, the confinement is the weakest with the longest distance of C-O (4.3 and 4.5 Å) and the lowest value of dominant peaks (1.38 and 1.42). Thus, it is found that confinement in tortuous channels is stronger than that in straight channel, which may further slows down the diffusion behaviors of methane.

3.6 | Extended discussion of limitations for diffusion simulation in the zeolite catalysts

In this work, the molecular dynamic simulation was used to determine the diffusion behavior of alkanes inside zeolite catalysts, and the dependence of zeolite topology on alkane diffusion inside nanochannels has been revealed. Therefore, our work has provided some theoretical methodologies and calculated models to estimate the relationship between the diffusion property and zeolite framework, and will benefits for the future design and practical applications of zeolite catalysts in the petrochemical industry.[79] But, it is noteworthy that the zeolite diffusion is very complicated under practical conditions, and the diffusion simulation is always restricted by the force-filed parameters. On one hand, the presence of heteroatoms (e.g., Si, Al, P, Ge and Ga) may have a significant effect on the diffusion inside real zeolites. For example, BOF is prone to incorporate Si, Al, Ge, Ga, and acid sites, while ATO, PON and PSI contains Si, Al, P and acid sites. It is worthwhile to note that an accurate and transferable force field which contains lots of heteroatoms is the most essential to determine the effect of heteroatoms on the diffusion. As well all know, the core-shell force field developed by Catlow et al is considerably most successful (for the accuracy and transferability) to describe the heteroatoms in the zeolites (e.g., Na, Mg, Al, Si, P, O and acid site),[48,49] and it has been demonstrated this force field could be reproduced structural properties and diffusion of zeolites with relatively smaller sizes.[80-83] However, it must be emphasized that the MD calculation with core-shell force field is a challenge since at least 10 times more computing time is demanded than other conventional nonpolarization force fields for the varied zeolite catalyst,[81-83] and thus it is difficult to be applied for the large zeolite system (i.e., ATO (6,912 atoms), PON (3,456 atoms), BOF (2,304 atoms), PSI (8,640 atoms), MFI (6,912 atoms) and MEL (6,912 atoms) in this work, see Table 1). In addition, the force field for Ge and Ga atoms is also not available in core-shell force field so far, which further strongly limits the application of this force field in the zeolites with heteroatoms.

On the other hand, the flexibility of the zeolite framework which contains the thermal coupling between molecules may plays a crucial role in the diffusion property of zeolite catalysts. It has been illustrated that the simulation with the rigid framework could appropriately describe the diffusion behaviors in the zeolite, but which was strongly correlated with the size of molecules and the pore size of zeolites.[35,82,84,85] In comparison, it is more generally accepted that higher diffusivities would be obtained when the framework was treated as flexible.[84,86,87] As aforementioned discussion, the force field is the key parameter for the MD simulation. It is indicated that the flexible force field was always exclusively used for some typical zeolite framework, and thus was considerably restricted to be applied

for other zeolites due to its poor transferability.[81] For example, it shows that the force field developed by Yamahara et al,[88] Pedone et al,[89] and Shi et al[90] can be specially used to describe the flexibility of SOF, FER, and MFI, respectively. In addition, the BKS force field could be used for aluminophosphates, while it was failed for MFI zeolite as it is ready to lead the distortion of the zeolite framework.[82] As there are varied topologies involved in our work, it is hard to ensure the specific force field could describe the flexibility of all the frameworks well. From this point of view, the rigid force field was still recommended to qualitatively simulate the diffusion behavior in zeolite catalysts so far.[50-53,82] The inherent problems of conventional MD simulation for the zeolite catalysts have been highlighted as aforementioned,[81] and it would prompt ongoing studies to develop an accurate, transferable and flexible force field to describe the flexibility of the framework and the component of zeolite (e.g., aluminosilicates, aluminophosphates, and other heteroatoms). And thus, it is expected that the diffusion dynamics (e.g., diffusion trajectory and diffusion coefficient) could be quantitatively determined under industrial conditions with the advanced force field parameters in the future.

4 | CONCLUSIONS

In summary, a combination of MD and MC simulations have been performed to systematically investigate the diffusion behaviors of short-chain alkanes in three kinds of zeolite catalysts, which possess 1-D straight (PSI, ATO), 1-D tortuous (PON, BOF), 3-D intersecting (MFI, MEL) channels with close window size, taking into account the influence of temperature, concentration, chain length, and mixtures.

In contrast to the diffusion behaviors of alkane with isotropy in the gas phase, the diffusion in zeolites catalysis is complicated and anisotropic due to the confinement of framework. The diffusion coefficient (D_s) of alkane in zeolites (10^{-7} to 10^{-10} m^2/s) is lower than that in the gas phase (10^{-5} m^2/s) by two to five orders of magnitude. In tortuous channels, D_s of alkane is slower than that in straight channels which is contributing to more frequent collision between the gas and zeolite frameworks. In 3-D intersecting channels, D_s is anisotropic and strongly dependent on each interconnected 1-D channels. In addition, D_s is more sensitive to temperature in tortuous channels than in straight channels. While the influence of concentration on diffusion is not significantly different in all the channels, which shows D_s slow down as loading increase. As for alkanes with different chain length in pure or mixture components, except the resonant diffusion, the longer the chain, the slower the diffusion is. It is also found that zeolites possess an intense concentration due to the strong adsorption effect on alkane. The concentration of alkane in zeolite is about 10–30 times higher than that in the gas phase at ambient condition. The high concentration aggregation and slow diffusion facilitate the participation of reactants in zeolite heterogeneous catalysis. From this perspective, understanding the effects of pore dimensionality on adsorbates diffusion in zeolite materials would help to improve the performance of separation as well as catalysis, and facilitate the design of novel porous materials.

ACKNOWLEDGMENTS

This work was supported by the National Natural Science Foundation of China (No. 21902180, 91645112, 21802164, 21991090, 21991092, and U1832148), Shanghai Rising-Star Program (18QB1404500), and Natural Science Foundation of Hubei Province of China (No. 2018CFA009), Key Research Program of Frontier Sciences, CAS (No. QYZDB-SSW-SLH026). The authors are grateful to SINOPEC Shanghai Research Institute of Petrochemical Technology (417012-4) and Shenzhen Cloud Computing Center for their support in computing facilities.

ORCID

Zhiqiang Liu https://orcid.org/0000-0003-2872-0125
Rajamani Krishna https://orcid.org/0000-0002-4784-8530
Kuan Huang https://orcid.org/0000-0003-1905-3017
Anmin Zheng https://orcid.org/0000-0001-7115-6510

REFERENCES

1. Kanezashi M, O'Brien-Abraham J, Lin YS, Suzuki K. Gas permeation through DDR-type zeolite membranes at high temperatures. *AIChE J*. 2008;54(6):1478-1486.
2. Tsapatsis M. 2-dimensional zeolites. *AIChE J*. 2014;60(7):2374-2381.
3. Li JR, Kuppler RJ, Zhou HC. Selective gas adsorption and separation in metal-organic frameworks. *Chem Soc Rev*. 2009;38(5):1477-1504.
4. Li Y, Yang RT. Hydrogen storage in metal-organic and covalent-organic frameworks by spillover. *AIChE J*. 2008;54(1):269-279.
5. Smit B, Maesen TLM. Towards a molecular understanding of shape selectivity. *Nature*. 2008;451(7179):671-678.
6. Krishna R, van Baten JM. Using molecular simulations for screening of zeolites for separation of CO_2/CH_4 mixtures. *Chem Eng J*. 2007;133(1–3):121-131.
7. Schenk M, Smit B, Vlugt TJH, Maesen TLM. Shape selectivity in hydrocarbon conversion. *Angew Chem Int Ed*. 2001;40(4):736-739.
8. Schuring D, Jansen APJ, van Santen RA. Concentration and chainlength dependence of the diffusivity of alkanes in zeolites studied with MD simulations. *J Phys Chem B*. 2000;104(5):941-948.
9. Epelde E, Aguayo AT, Olazar M, Bilbao J, Gayubo AG. Kinetic model for the transformation of 1-butene on a k-modified HZSM-5 catalyst. *Ind Eng Chem Res*. 2014;53(26):10599-10607.
10. Tan Q, Fan Y, Liu H, et al. Bimodal micro-mesoporous aluminosilicates for heavy oil cracking: porosity tuning and catalytic properties. *AIChE J*. 2008;54(7):1850-1859.
11. Macht J, Carr RT, Iglesia E. Consequences of acid strength for isomerization and elimination catalysis on solid acids. *J Am Chem Soc*. 2009;131(18):6554-6565.
12. Baerlocher, C.; McCusker, L. B. Database of Zeolite Structures. Available at http://www.iza-structure.org/databases/ (Accessed Jun 2016).
13. Beerdsen E, Dubbeldam D, Smit B. Understanding diffusion in nanoporous materials. *Phys Rev Lett*. 2006;96(4):044501.
14. Ackley MW, Rege SU, Saxena H. Application of natural zeolites in the purification and separation of gases. *Microporous Mesoporous Mater*. 2003;61(1–3):25-42.
15. Smit B, Maesen TLM. Molecular simulations of zeolites: adsorption, diffusion, and shape selectivity. *Chem Rev*. 2008;108(10):4125-4184.
16. Ahn JH, Kolvenbach R, Gutiérrez OY, Al-Khattaf SS, Jentys A, Lercher JA. Tailoring p-xylene selectivity in toluene methylation on medium pore-size zeolites. *Microporous Mesoporous Mater*. 2015;210:52-59.
17. Baumgärtl M, Jentys A, Lercher JA. Understanding elementary steps of transport of xylene mixtures in ZSM-5 zeolites. *J Phys Chem C*. (accpeted). 2019;123:8092–8100.

18. Shen Y, Le TT, Fu D, et al. Deconvoluting the competing effects of zeolite framework topology and diffusion path length on methanol to hydrocarbons reaction. *ACS Catal*. 2018;8(12):11042-11053.
19. Liu Z, Yi X, Wang G, et al. Roles of 8-ring and 12-ring channels in mordenite for carbonylation reaction: from the perspective of molecular adsorption and diffusion. *J Catal*. 2019;369:335-344.
20. Centi G, Perathoner S. Catalysis: role and challenges for a sustainable energy. *Top Catal*. 2009;52(8):948-961.
21. Zaera F. New challenges in heterogeneous catalysis for the 21st century. *Catal Lett*. 2012;142(5):501-516.
22. Van Speybroeck V, Hemelsoet K, Joos L, Waroquier M, Bell RG, Catlow CRA. Advances in theory and their application within the field of zeolite chemistry. *Chem Soc Rev*. 2015;44(20):7044-7111.
23. Jobic H, Schmidt W, Krause CB, Karger J. PFG NMR and QENS diffusion study of n-alkane homologues in MFI-type zeolites. *Microporous Mesoporous Mater*. 2006;90(1–3):299-306.
24. Jobic H, Theodorou DN. Diffusion of long n-alkanes in silicalite. A comparison between neutron scattering experiments and hierarchical simulation results. *J Phys Chem B*. 2006;110(5):1964-1967.
25. Hendriks FC, Meirer F, Kubarev AV, et al. Single-molecule fluorescence microscopy reveals local diffusion coefficients in the pore network of an individual catalyst particle. *J Am Chem Soc*. 2017;139(39):13632-13635.
26. Zuerner A, Kirstein J, Doeblinger M, Braeuchle C, Bein T. Visualizing single-molecule diffusion in mesoporous materials. *Nature*. 2007;450(7170):705-708.
27. Rittig F, Farris TS, Zielinski JM. Predicting packed-bed breakthrough behavior from PFG NMR diffusion data. *AIChE J*. 2004;50(3):589-595.
28. Skoulidas AI, Sholl DS. Molecular dynamics simulations of self-diffusivities, corrected diffusivities, and transport diffusivities of light gases in four silica zeolites to assess influences of pore shape and connectivity. *J Phys Chem A*. 2003;107(47):10132-10141.
29. Sholl DS. Understanding macroscopic diffusion of adsorbed molecules in crystalline nanoporous materials via atomistic simulations. *Acc Chem Res*. 2006;39(6):403-411.
30. Krishna R. Describing the diffusion of guest molecules inside porous structures. *J Phys Chem C*. 2009;113(46):19756-19781.
31. Ghysels A, Moors SLC, Hemelsoet K, et al. Shape-selective diffusion of olefins in 8-ring solid acid microporous zeolites. *J Phys Chem C*. 2015;119(41):23721-23734.
32. Krishna R, van Baten JM. A molecular dynamic investigation of the diffusion of methane-ethane and methane-propane mixtures in zeolites. *Chem Eng Technol*. 2006;29(12):1429-1437.
33. Garcia-Perez E, Parra JB, Ania CO, et al. A computational study of CO_2, N_2, and CH_4 adsorption in zeolites. *Adsorption*. 2007;13(5–6):469-476.
34. Krishna R, van Baten JM. A molecular dynamics investigation of a variety of influences of temperature on diffusion in zeolites. *Microporous Mesoporous Mater*. 2009;125(1):126-134.
35. Krishna R, van Baten JM. A molecular dynamics investigation of the diffusion characteristics of cavity-type zeolites with 8-ring windows. *Microporous Mesoporous Mater*. 2011;137(1–3):83-91.
36. Beerdsen E, Dubbeldam D, Smit B. Molecular understanding of diffusion in confinement. *Phys Rev Lett*. 2005;95(16):164505.
37. Dubbeldam D, Beerdsen E, Calero S, Smit B. Molecular path control in zeolite membranes. *P Natl Acad Sci USA*. 2005;102(35):12317-12320.
38. Kubu M, Zilkova N, Zones SI, Chen CY, Al-Khattaf S, Cejka J. Three-dimensional 10-ring zeolites: the activities in toluene alkylation and disproportionation. *Catal Today*. 2016;259:97-106.
39. Bleken F, Skistad W, Barbera K, et al. Conversion of methanol over 10-ring zeolites with differing volumes at channel intersections: comparison of TNU-9, IM-5, ZSM-11 and ZSM-5. *Phys Chem Chem Phys*. 2011;13(7):2539-2549.
40. Narbeshuber TF, Brait A, Seshan K, Lercher JA. Dehydrogenation of light alkanes over zeolites. *J Catal*. 1997;172(1):127-136.
41. Janda A, Bell AT. Effects of si/al ratio on the distribution of framework al and on the rates of alkane monomolecular cracking and dehydrogenation in H-MFI. *J Am Chem Soc*. 2013;135(51):19193-19207.
42. Olsbye U, Svelle S, Bjorgen M, et al. Conversion of methanol to hydrocarbons: how zeolite cavity and pore size controls product selectivity. *Angew Chem Int Ed*. 2012;51(24):5810-5831.
43. Rahimi N, Karimzadeh R. Catalytic cracking of hydrocarbons over modified ZSM-5 zeolites to produce light olefins: a review. *Appl Catal A Gen*. 2011;398(1–2):1-17.
44. Akhmedov VM, Al-Khowaiter SH. Recent advances and future aspects in the selective isomerization of high n-alkanes. *Catal Rev Sci Eng*. 2007;49(1):33-139.
45. Bhasin MM, McCain JH, Vora BV, Imai T, Pujado PR. Dehydrogenation and oxydehydrogenation of paraffins to olefins. *Appl Catal A Gen l*. 2001;221(1–2):397-419.
46. Martens GG, Marin GB. Kinetics for hydrocracking based on structural classes: model development and application. *AIChE J*. 2001;47(7):1607-1622.
47. Gale JD, Rohl AL. The general utility lattice program (GULP). *Mol Simul*. 2003;29(5):291-341.
48. Schroder KP, Sauer J, Leslie M, Catlow CRA, Thomas JM. Bridging hydroxyl-groups in zeolitic catalysts - a computer-simulation of their structure, vibrational properties and acidity in protonated faujasites (H-Y zeolites). *Chem Phys Lett*. 1992;188(3–4):320-325.
49. Sanders MJ, Leslie M, Catlow CRA. Interatomic potentials for SiO_2. *J Chem Soc Chem Commun*. 1984;19:1271-1273.
50. Dubbeldam D, Calero S, Vlugt TJH, Krishna R, Maesen TLM, Smit B. United atom force field for alkanes in nanoporous materials. *J Phys Chem B*. 2004;108(33):12301-12313.
51. Yang CT, Janda A, Bell AT, Lin LC. Atomistic investigations of the effects of Si/Al ratio and Al distribution on the adsorption selectivity of n-alkanes in Brønsted acid zeolites. *J Phys Chem C*. 2018;122(17):9397-9410.
52. Slawek A, Vicent-Luna JM, Ogorzaly K, et al. Adsorption of alkanes in zeolites LTA and FAU: quasi-equilibrated thermodesorption supported by molecular simulations. *J Phys Chem C*. 2019;123(49):29665-29678.
53. Slawek A, Vicent-Luna JM, Marsalek B, Balestra SRG, Makowski W, Calero S. Adsorption of n-alkanes in MFI and MEL: quasi-equilibrated Thermodesorption combined with molecular simulations. *J Phys Chem C*. 2016;120(44):25338-25350.
54. Chib S, Greenberg E. Understanding the metropolis-Hastings algorithm. *Am Stat*. 1995;49(4):327-335.
55. Widom B. Some topics in theory of fluids. *J Chem Phys*. 1963;39(11):2808-2818.
56. Martyna GJ, Klein ML, Tuckerman M. Nose-hoover chains - the canonical ensemble via continuous dynamics. *J Chem Phys*. 1992;97(4):2635-2643.
57. Van Gunsteren WF, Berendsen HJC. A leap-frog algorithm for stochastic dynamics. *Mol Simul*. 1988;1(3):173-185.
58. Dubbeldam D, Calero S, Ellis DE, Snurr RQ. RASPA: molecular simulation software for adsorption and diffusion in flexible nanoporous materials. *Mol Simul*. 2016;42(2):81-101.
59. Smith W, Forester TR. DL_POLY_2.0: a general-purpose parallel molecular dynamics simulation package. *J Mol Graph*. 1996;14(3):136-141.
60. Frenkel D, Smit B. *Understanding molecular simulations*. 2nd ed. Elsevier: Academic Press; 2002.
61. Kleinrahm R, Duschek W, Wagner W, Jaeschke M. Measurement and correlation of the (pressure, density, temperature) relation of methane in the temperature-range from 273.15 k to 323.15 K at pressures up to 8 Mpa. *J Chem Thermodyn*. 1988;20(5):621-631.
62. Murata K, Miyawaki J, Yudasaka M, Iijima S, Kaneko K. High-density of methane confined in internal nanospace of single-wall carbon nanohorns. *Carbon*. 2005;43(13):2826-2830.

63. Higgoda UA, Hellmann R, Koller TM, Fröba AP. Self-diffusion coefficient and viscosity of methane and carbon dioxide via molecular dynamics simulations based on new ab initio-derived force fields. *Fluid Phase Equilib*. 2019;481:15-27.
64. Sholl DS, Lively RP. Seven chemical separations to change the world. *Nature*. 2016;532(7600):435-437.
65. Krishna R, van Baten JM. Insights into diffusion of gases in zeolites gained from molecular dynamics simulations. *Microporous Mesoporous Mater*. 2008;109(1–3):91-108.
66. Runnebaum RC, Maginn EJ. Molecular dynamics simulations of alkanes in the zeolite silicalite: evidence for resonant diffusion effects. *J Phys Chem B*. 1997;101(33):6394-6408.
67. Yoo K, Tsekov R, Smirniotis PG. Experimental proof for resonant diffusion of normal alkanes in LTL and ZSM-12 zeolites. *J Phys Chem B*. 2003;107(49):13593-13596.
68. Ban S, Vlugt TJH. Adsorption and diffusion of alkanes in Na-MOR: modeling the effect of the aluminum distribution. *J Chem Theory Comput*. 2009;5(10):2858-2865.
69. Hong U, Kärger J, Kramer R, et al. PFG N.M.R. study of diffusion anisotropy in oriented ZSM-5 type zeolite crystallites. *Zeolites*. 1991;11(8):816-821.
70. Jeon MY, Kim D, Kumar P, et al. Ultra-selective high-flux membranes from directly synthesized zeolite nanosheets. *Nature*. 2017;543(7647):690-694.
71. Krishna R. Diffusion in porous crystalline materials. *Chem Soc Rev*. 2012;41(8):3099-3118.
72. Krishna R. Occupancy dependency of Maxwell-Stefan diffusivities in ordered crystalline microporous materials. *ACS Omega*. 2018;3(11):15743-15753.
73. Liu Z, Chu Y, Tang X, et al. Diffusion dependence of the dual-cycle mechanism for mto reaction inside ZSM-12 and ZSM-22 zeolites. *J Phys Chem C*. 2017;121(41):22872-22882.
74. Toda J, Sastre G. Diffusion of trimethylbenzenes, toluene, and xylenes in UWY zeolite as a catalyst for transalkylation of trimethylbenzenes with toluene. *J Phys Chem C*. 2018;122(14):7885-7897.
75. Balucani U, Brodholt JP, Vallauri R. Analysis of the velocity autocorrelation function of water. *J Phys Condens Matter*. 1996;8(34):6139-6144.
76. Weber SC, Thompson MA, Moerner WE, Spakowitz AJ, Theriot JA. Analytical tools to distinguish the effects of localization error, confinement, and medium elasticity on the velocity autocorrelation function. *Biophys J*. 2012;102(11):2443-2450.
77. Mitra S, Sharma VK, Chaplot SL, Mukhopadhyay R. Diffusion of hydrocarbon in zeolite and effect due to pore topology: neutron scattering and MD simulation studies. *Chem Phys*. 2014;430:69-77.
78. Findley JM, Ravikovitch PI, Sholl DS. The effect of aluminum short-range ordering on carbon dioxide adsorption in zeolites. *J Phys Chem C*. 2018;122(23):12332-12340.
79. Shi J, Wang YD, Yang WM, Tang Y, Xie ZK. Recent advances of pore system construction in zeolite-catalyzed chemical industry processes. *Chem Soc Rev*. 2015;44(24):8877-8903.
80. Combariza AF, Gomez DA, Sastre G. Simulating the properties of small pore silica zeolites using interatomic potentials. *Chem Soc Rev*. 2013;42(1):114-127.
81. Dubbeldam D, Walton KS, Vlugt TJH, Calero S. Design, parameterization, and implementation of atomic force fields for adsorption in nanoporous materials. *Adv Theory Simul*. 2019;2(11):1900135.
82. Toda J, Corma A, Abudawoud RH, Elanany MS, Al-Zahrani IM, Sastre G. Influence of force fields on the selective diffusion of Para-xylene over ortho-xylene in 10-ring zeolites. *Mol Simul*. 2015;41(16–17):1438-1448.
83. Toda J, Corma A, Sastre G. Diffusion of trimethylbenzenes and xylenes in zeolites with 12- and 10-ring channels as catalyst for toluene-trimethylbenzene transalkylation. *J Phys Chem C*. 2016;120(30):16668-16680.
84. Leroy F, Rousseau B, Fuchs AH. Self-diffusion of n-alkanes in silicalite using molecular dynamics simulation: a comparison between rigid and flexible frameworks. *Phys Chem Chem Phys*. 2004;6(4):775-783.
85. Fritzsche S, Wolfsberg M, Haberlandt R, Demontis P, Suffritti GB, Tilocca A. About the influence of lattice vibrations on the diffusion of methane in a cation-free LTA zeolite. *Chem Phys Lett*. 1998;296(3–4):253-258.
86. Garcia-Sanchez A, Dubbeldam D, Calero S. Modeling adsorption and self-diffusion of methane in LTA zeolites: the influence of framework flexibility. *J Phys Chem C*. 2010;114(35):15068-15074.
87. Kopelevich DI, Chang HC. Diffusion of inert gases in silica sodalite: importance of lattice flexibility. *J Chem Phys*. 2001;115(20):9519-9527.
88. Yamahara K, Okazaki K, Kawamura K. Molecular-dynamics studies on thermal-behavior of an MFI-type zeolite. *Catal Today*. 1995;23(4):397-11253.
89. Pedone A, Malavasi G, Menziani MC, Cormack AN, Segre U. A new self-consistent empirical interatomic potential model for oxides, silicates, and silica-based glasses. *J Phys Chem B*. 2006;110(24):11780-11795.
90. Shi HB, Migues AN, Auerbach SM. Ab initio and classical simulations of the temperature dependence of zeolite pore sizes. *Green Chem*. 2014;16(2):875-884.

SUPPORTING INFORMATION

Additional supporting information may be found online in the Supporting Information section at the end of this article.

How to cite this article: Liu Z, Zhou J, Tang X, et al. Dependence of zeolite topology on alkane diffusion inside diverse channels. *AIChE Journal*. 2020;66:e16269. https://doi.org/10.1002/aic.16269

Supporting Information

Dependence of Zeolite Topology on Alkane Diffusion inside Nano-Channels

Zhiqiang Liu[a], Jian Zhou[b] , Xiaomin Tang[a,c] , Fujian Liu[d], Jiamin Yuan[a,c], Guangchao Li[a,c], Ling Huang[a], Rajamani Krishna[e], Kuan Huang[f,*], Anmin Zheng[a,*]

[a] State Key Laboratory of Magnetic Resonance and Atomic and Molecular Physics, National Center for Magnetic Resonance in Wuhan, Wuhan Institute of Physics and Mathematics, Innovation Academy for Precision Measurement Science and Technology, Chinese Academy of Sciences, Wuhan 430071, P.R. China.

[b] Shanghai Research Institute of Petrochemical Technology, SINOPEC, Shanghai 201208, P.R. China.

[c] University of Chinese Academy of Sciences, Beijing 100049, P. R. China.

[d] National Engineering Research Center for Chemical Fertilizer Catalyst (NERC-CFC), School of Chemical Engineering, Fuzhou University, Fuzhou 350116, P. R. China.

[e] Van't Hoff Institute for Molecular Sciences, University of Amsterdam, Science Park 904, 1098 XH Amsterdam, The Netherlands.

[f] Key Laboratory of Poyang Lake Environment and Resource Utilization of Ministry of Education, School of Resources Environmental and Chemical Engineering,

Nanchang University, Nanchang 330031, P. R. China.

* Corresponding authors: huangk@ncu.edu.cn; zhenganm@wipm.ac.cn.

1. Validity of force field

First of all, the SLC core-shell force field [1] which gives an accurate description of the thermal expansion behavior [2] was used to investigate the effect of thermal coupling for the lattice. It shows negative thermal expansion as Shi[3] and Tschaufeser's work[4]. However, the changes of volume are very small for MFI (See Table S1), which was respectively about 0.33%, 0.42% and 0.76% at 300, 600 and 900 K smaller than that at 0 K (DFT optimizing). Thus, we did not consider the thermal expansion in this work.

Furthermore, we have also compared the heat of adsorption and self-diffusion coefficient (*Ds*) with experimental value. The heat of adsorption of methane in MFI zeolites is 17.6 kj/mol, which is consisted with that 16 ± 4 kj/mol in experiment. [6,7] D_s for methane diffusion at 300 K in MFI were about 0.7 to 1.4 × 10^{-8} m^2/s from 1 to 6 per unit, which were consisted with that for PFG-NMR method of Caro *et al.* 1.1 ± 0.55 × 10^{-8} m^2/s. [8,9] Besides the rigid force field have been widely used in some other work. [10-13] Overall, it's confirmed that the force field could be used to investigate the adsorption and diffusion for hydrocarbon inside zeolites.

The parameters of the force field are taken from Dubbeldam's work [10] and the Lennar-Jones parameters are also shown (See Table S2).

Table S1. Changes of volume for MFI (1×2×1 super cell) zeolite at various temperature.

Temperature (K)	Volume ($Å^3$)	Changes of volume
0	10551	-
300	10517	-0.33%
600	10507	-0.42%
900	10471	-0.76%

Table S2. Lennard-Jones Parameters [a]

	O	CH_4	CH_3	CH_2
CH_4	115.00	158.50	130.84	94.21
	3.47	3.72	3.74	3.84
CH_3	93.00	130.84	108.00	77.77
	3.48	3.74	3.76	3.86
CH_2	60.50	94.21	77.77	56.00
	3.58	3.84	3.86	3.96

[a] Lennard-Jones parameters, ε/kB [K] in top, σ [Å] in bottom of each field.

References

1. Sanders MJ, Leslie M, Catlow CRA. Interatomic potentials for SiO2. *J Chem Soc Chem Commun.* 1984;(19):1271-1273.

2. Martinez-Inesta MM, Lobo, RF. Investigation of the negative thermal expansion mechanism of zeolite Chabazite using the pair distribution function method. *J Phys Chem B*. 2005;109(19): 9389-9396.

3. Shi HB, Migues AN, Auerbach SM. Ab initio and classical simulations of the temperature dependence of zeolite pore sizes. *Green Chem.* 2014;16(2): 875-884

4. Tschaufese P, Parker SC. Thermal expansion behavior of zeolites and $AlPO_4$s. *J Phys Chem.* 1995;99(26): 10609-10615.

5. Otto K, Montreuil CN, Todor O *et al*. Adsorption of hydrocarbons and other exhaust components on Silicalite. *Ind Eng Chem Res.* 1991;30(10):2333-2340.

6. Choudhary VR, Mayadevi S. Adsorption of methane, ethane, ethylene, and carbon dioxide on high Silica pentasil zeolites and zeolite-like materials using gas chromatography pulse technique. *Sep Sci Technol.* 1993;28(13-14):2197-220.

7. Nicholas JB, Trouw FR, Mertz JE *et al*. Molecular dynamics simulation of propane and methane in Silicalite. *J Phys Chem.* 1993; 97(16): 4149-4163.

8. Caro J, Bulow M, Schirmer W *et al*. Microdynamics of methane, ethane and propane in ZSM-5 type zeolites. *J Chem Soc Faraday Trans I.* 1985; 81:2541-2550.

9. Dubbeldam D, Calero S, Vlugt TJH, Krishna R, Maesen TLM, Smit B. United atom force field for alkanes in nanoporous materials. *J Phys Chem B.* 2004;108(33):12301-12313.

10. Yang CT, Janda A, Bell AT, Lin LC. Atomistic investigations of the effects of Si/Al ratio and Al distribution on the adsorption selectivity of n‑alkanes in Brønsted acid zeolites. *J Phys Chem C*. 2018; 122(17):9397-9410.

11. Slawek A, Vicent-Luna JM, Ogorzaly K, Valencia S, Rey F, Makowski W, Calero S. Adsorption of alkanes in zeolites LTA and FAU: Quasi-equilibrated

thermodesorption supported by molecular simulations. *J Phys Chem C.* 2019; 123(49):29665−29678.

12. Slawek A, Vicent-Luna JM, Marsalek B, Balestra SRG, Makowski W, Calero S. Adsorption of n‑alkanes in MFI and MEL: Quasi-Equilibrated Thermodesorption combined with molecular simulations. *J Phys Chem C.* 2016;120(44):25338-25350.

2. Diffusion coefficients

Table S3. Diffusion coefficients (D) of alkanes in the x (D_x), y (D_y) and z (D_z) directions. D_s represents the average diffusion coefficients for three directions (see **Figure 4** in the paper)

(a) Diffusion coefficients (D) of methane at 1 atm, as a function of temperature.

Temperature/(K)	Diffusion coefficients (D) / (10^{-5} m^2/s)			
	D_x	D_y	D_z	D_s
300	2.2	2.2	2.2	2.2
450	3.1	3.2	3.0	3.1
600	7.6	7.6	7.8	7.6
750	10.7	11.0	10.6	10.8
900	15.1	14.7	14.9	14.9

(b) Diffusion coefficients (D) of methane at 300 K, as a function of pressure.

Pressure/(atm)	Diffusion coefficients (D) / (10^{-5} m^2/s)			
	D_x	D_y	D_z	D_s
0.5	4.2	4.3	4.2	4.2
1.0	2.2	2.2	2.2	2.2

5.0	0.4	0.5	0.5	0.5
10.0	0.2	0.2	0.2	0.2
20.0	0.1	0.1	0.1	0.1

(c) Diffusion coefficients (*D*) of methane (C1), ethane (C2), propane (C3) and *n*-butane (C4) at ambient conditions (*i.e.* 1 atm and 300 K).

Alkane	Diffusion coefficients (D) / (10^{-5} m^2/s)			
	D_x	D_y	D_z	D_s
C1	2.2	2.2	2.2	2.2
C2	1.3	1.4	1.3	1.3
C3	1.0	1.0	1.0	1.0
C4	0.6	0.6	0.6	0.6

(d) Diffusion coefficients (*D*) of C1-Cn mixtures (ratio of 1:1, n = 1 - 4) at ambient conditions.

Mixture	Alkane	Diffusion coefficients (D) / (10^{-5} m^2/s)			
		D_x	D_y	D_z	D_s
C1 - C1	C1	2.2	2.2	2.2	2.2

	C1	2.2	2.2	2.2	2.2
C1 - C2	C1	2.3	2.2	2.2	2.2
	C2	1.5	1.6	1.5	1.5
C1 - C3	C1	2.3	2.1	2.4	2.3
	C3	1.3	1.1	1.3	1.2
C1 - C4	C1	2.3	2.1	2.3	2.2
	C4	0.9	0.9	0.9	0.9

Table S4. Diffusion coefficients (D_s) of alkanes inside 1-D channels of BOF, PON, PSI and ATO zeolites (see **Figure 5** in the paper).

(a) Diffusion coefficients (D_s) of methane at infinite dilution, as a function of temperature.

Temperature/(K)	Diffusion coefficients (D_s) / (10^{-10} m^2/s)			
	BOF	PON	PSI	ATO
300	4.3 ± 0.3	59.3 ± 1.6	185.7 ± 17.6	1868.6 ± 125.7
450	12.6 ± 0.8	143.6 ± 7.2	395.8 ± 24.6	2401.0 ± 127.2
600	19.0 ± 1.4	219.3 ± 4.7	558.2 ± 36.2	3073.1 ± 222.0
750	30.6 ± 1.4	276.0 ± 16.9	591.1 ± 30.8	3469.9 ± 238.2
900	40.0 ± 5.0	313.1 ± 10.9	671.5 ± 39.2	3813.9 ± 262.4

(b) Diffusion coefficients (D_s) of methane at 300 K, as a function of loading.

Alkane	Diffusion coefficients (D_s) / (10^{-10} m^2/s)			
	BOF	PON	PSI	ATO
C1	4.3 ± 0.3	59.3 ± 1.6	185.7 ± 17.6	1868.6 ± 125.7

C2	3.7 ± 0.3	44.1 ± 1.4	69.3 ± 3.2	426.9 ± 37.9
C3	9.2 ± 0.8	8.6 ± 0.4	95.4 ± 10.0	521.0 ± 15.2
C4	1.3 ± 0.1	6.4 ± 0.4	241.5 ± 21.2	1089.0 ± 57.7

(c) Diffusion coefficients (D_s) of methane (C1), ethane (C2), propane (C3) and *n*-butane (C4) at infinite dilution and 300 K.

Loading / (molecules/super cell)	Diffusion coefficients (D_s) / (10^{-10} m^2/s)			
	BOF	PON	PSI	ATO
16	4.3 ± 0.3	-	185.7 ± 17.6	-
24	-	59.3 ± 1.6	-	1868.6 ± 125.7
32	2.0 ± 0.1	-	99.3 ± 6.5	-
48	-	30.6 ± 1.6	-	1017.7 ± 38.5
64	0.8 ± 0.0	-	39.3 ± 2.8	-
96	0.2 ± 0.0	8.0 ± 0.3	16.1 ± 1.0	302.7 ± 19.5
144	-	2.1 ± 0.1	-	144.6 ± 7.7

(d) Diffusion coefficients (D_s) of mixtures with methane and other alkane molecules

at 1:1 loading and 300 K. D_s of Cx_{Cy} (x = 1 - 4, y = 1 - 4) represents the diffusion coefficients of Cx when mixed with Cy.

Mixture	Diffusion coefficients (D_s) / (10^{-10} m^2/s)			
	BOF	PON	PSI	ATO
$C1_{C1}$	2.0 ± 0.1	30.6 ± 1.6	99.3 ± 6.5	1017.7 ± 38.5
$C1_{C2}$	2.2 ± 0.3	24.9 ± 2.0	58.6 ± 10.3	564.8 ± 74.4
$C1_{C3}$	3.3 ± 0.2	18.4 ± 4.6	85.5 ± 6.5	593.7 ± 70.7
$C1_{C4}$	1.5 ± 0.2	7.7 ± 1.1	84.7 ± 5.2	710.2 ± 15.5
$C2_{C1}$	2.1 ± 0.2	20.7 ± 0.9	48.3 ± 2.5	327.5 ± 25.1
$C3_{C1}$	4.3 ± 0.2	6.2 ± 0.5	70.8 ± 3.2	359.1 ± 16.7
$C4_{C1}$	0.7 ± 0.0	4.9 ± 0.3	92.4 ± 9.1	532.6 ± 19.6

Table S5. Diffusion coefficients (D_s) of alkanes inside MFI and MEL zeolites in the x (red), y (green), and z (blue) directions (see **Figure 8** in the paper).

(a) Diffusion coefficients (D_s) of methane at infinite dilution, as a function of temperature.

Temperature/	MFI			MEL		
(K)	D_x	D_y	D_z	D_x	D_y	D_z

300	150.6 ± 5.4	234.9 ± 6.1	30.6 ± 1.5	216.0 ± 8.6	222.2 ± 7.9	21.1 ± 0.6
450	246.3 ± 15.2	362.2 ± 6.9	49.9 ± 1.9	379.0 ± 19.6	360.4 ± 11.3	36.6 ± 1.2
600	340.0 ± 9.0	524.6 ± 15.8	60.0 ± 3.4	496.0 ± 17.5	549.0 ± 10.7	49.2 ± 0.4
750	404.5 ± 15.1	659.8 ± 16.8	77.6 ± 3.8	635.3 ± 23.0	639.7 ± 19.5	54.8 ± 2.5
900	420.9 ± 17.9	695.3 ± 23.1	87.8 ± 2.2	650.2 ± 26.8	796.5 ± 23.6	68.9 ± 2.6

(b) Diffusion coefficients (D_s) of methane at 300 K, as a function of loading.

Loading/ (molecules/ super cell)	MFI			MEL		
	D_x	D_y	D_z	D_x	D_y	D_z
24	150.6 ± 5.4	234.9 ± 6.1	30.6 ± 1.5	216.0 ± 8.6	222.2 ± 7.9	21.1 ± 0.6
48	135.0 ± 3.1	210.8 ± 6.5	28.3 ± 0.8	202.7 ± 6.1	197.5 ± 7.4	22.3 ± 0.9
96	104.8 ± 1.8	167.5 ± 1.9	24.6 ± 0.1	149.6 ± 4.3	150.0 ± 2.0	18.1 ± 0.3
144	79.8 ± 1.5	123.2 ± 2.2	18.9 ± 0.3	116.9 ± 1.9	113.4 ± 2.9	15.3 ± 0.2

(c) Diffusion coefficients (D_s) of methane (C1), ethane (C2), propane (C3) and *n*-butane (C4) at infinite dilution and 300 K.

Alkane	MFI			MEL		
	D_x	D_y	D_z	D_x	D_y	D_z
C1	150.6 ± 5.4	234.9 ± 6.1	30.6 ± 1.5	216.0 ± 8.6	222.2 ± 7.9	21.1 ± 0.6
C2	77.2 ± 3.8	134.2 ± 1.1	15.5 ± 0.5	118.6 ± 3.3	112.1 ± 4.1	10.6 ± 0.3
C3	41.2 ± 1.2	71.4 ± 3.2	10.1 ± 0.4	73.7 ± 2.2	75.9 ± 4.3	9.8 ± 0.2
C4	23.8 ± 0.5	72.6 ± 4.0	6.4 ± 0.3	80.7 ± 2.9	77.6 ± 5.6	6.3 ± 0.3

(d) D_s of mixtures with 24 methane and 24 other alkane molecules at 300 K.

Mixture	MFI			MEL		
	D_x	D_y	D_z	D_x	D_y	D_z
$C1_{C1}$	135.0 ± 3.1	210.8 ± 6.5	28.3 ± 0.8	202.7 ± 6.1	197.5 ± 7.4	22.3 ± 0.9
$C1_{C2}$	120.9 ± 3.9	215.5 ± 6.9	26.2 ± 1.1	178.3 ± 10.1	188.9 ± 2.5	19.3 ± 0.8
$C1_{C3}$	104.5 ± 5.7	168.4 ± 2.8	24.8 ± 0.6	177.2 ± 5.3	170.4 ± 9.5	20.3 ± 0.4
$C1_{C4}$	110.8 ± 2.5	151.1 ± 6.0	21.8 ± 1.0	167.5 ± 3.6	180.5 ± 4.1	17.3 ± 0.4
$C2_{C1}$	74.8 ± 2.8	115.2 ± 5.2	15.0 ± 0.9	101.6 ± 6.1	95.8 ± 1.9	10.2 ± 0.4

$C3_{C1}$	38.5 ± 0.8	72.3 ± 3.2	9.4 ± 0.2	67.8 ± 3.2	67.4 ± 2.1	10.3 ± 0.5
$C4_{C1}$	22.2 ± 1.1	71.5 ± 2.9	6.2 ± 0.2	73.3 ± 1.5	74.6 ± 0.8	6.6 ± 0.4

3. Estimation of self-diffusivities in binary mixtures

Binary mixture diffusion in nano-sized channels of zeolites is characterized by the fact that the mobility of any guest constituent is influenced by its partner species;[1,2] the proper modelling of such influences is essential for process development and design.[3,4] It is common practice to model binary mixture diffusion by adopting the Maxwell-Stefan (M-S) formulation,[4-9] that has its foundations in the theory of non-equilibrium thermodynamics. The dependence of the intra-crystalline molar fluxes N_i on the chemical potential gradients is written in the following form

$$-\frac{\rho q_1}{RT}\frac{d\mu_1}{dz} = \frac{x_2 N_1 - x_1 N_2}{Đ_{12}} + \frac{N_1}{Đ_1}$$
$$-\frac{\rho q_1}{RT}\frac{d\mu_2}{dz} = \frac{x_1 N_2 - x_2 N_1}{Đ_{21}} + \frac{N_2}{Đ_2} \quad (1)$$

In eq **Error! Reference source not found.**, R is the gas constant, □ represents the material framework density, and the component loadings q_i are defined in terms of moles per kg of framework material. The x_i in eq **Error! Reference source not found.** are the mole fractions of the adsorbed phase components

$$x_i = \frac{q_i}{q_t}; q_t = q_1 + q_2; i = 1,2 \quad (2)$$

Two distinct sets of M-S diffusivities are defined by eq **Error! Reference source not found.**, that is phenomenological in nature.[10] The $Đ_i$ characterize interactions between species i with the pore walls. As established in earlier works,[7,9,11,12] the important advantage of the M-S formulation is that the $Đ_1$ and $Đ_2$ can be identified with

the corresponding unary diffusivities, provided the diffusivity data are compared at the total loading. For unary diffusion, the $Đ_i$ are determinable from MD simulations of molecular displacements using the formula in each of the coordinate direction

$$Đ_i = \frac{1}{2}\lim_{\Delta t\to\infty}\frac{1}{n_i}\frac{1}{\Delta t}\left\langle\left(\sum_{l=1}^{n_i}\left(\mathbf{r}_{l,i}(t+\Delta t)-\mathbf{r}_{l,i}(t)\right)\right)^2\right\rangle \tag{3}$$

The exchange coefficients, $Đ_{12}$, and $Đ_{21}$ defined by the first right members of eq **Error! Reference source not found.** reflect how the facility for transport of species 1 *correlates* with that of species 2. The Onsager reciprocal relations impose the symmetry constraint

$$Đ_{12} = Đ_{21} \tag{4}$$

The magnitude of $Đ_1$ relative to that of $Đ_{12}$ determines the extent to which the flux of species 1 is influenced by the chemical potential gradient of species 2. The larger the *degree of correlations*, $Đ_1/Đ_{12}$, the stronger is the influence of diffusional "coupling". Generally speaking, the more-strongly-adsorbed-tardier partner species will have the effect of slowing down the less-strongly-adsorbed-more-mobile partner in the mixture.

Applying eq **Error! Reference source not found.** to a binary mixture consisting of tagged and untagged species *i*, that are otherwise identical,[5,13,14] we can derive the following relation between the unary self-diffusivity, $D_{i,self}$ and the M-S diffusivity $Đ_i$

$$\frac{1}{D_{i,self}} = \frac{1}{Đ_i} + \frac{1}{Đ_{ii}} \tag{5}$$

The self-diffusivities $D_{\mathrm{i,self}}$ may be computed from MD simulations by analyzing the mean square displacement of each species *i* for each coordinate direction[5]

$$D_{i,self} = \frac{1}{2n_i} \lim_{\Delta t \to \infty} \frac{1}{\Delta t} \left\langle \left(\sum_{l=1}^{n_i} \left(\mathbf{r}_{l,i}(t + \Delta t) - \mathbf{r}_{l,i}(t) \right)^2 \right) \right\rangle \tag{1}$$

The self-exchange coefficient $Đ_{\mathrm{ii}}$ can be determined from eq **Error! Reference source not found.** from MD simulation data for $Đ_{\mathrm{i}}$ and $D_{\mathrm{i,self}}$.

For estimation of the exchange coefficient, $Đ_{12}$, the following interpolation formula has been suggested in the literature[7,15]

$$Đ_{12} = Đ_{11}^{x_1} Đ_{22}^{x_2} \tag{7}$$

where the $Đ_{11}$ and $Đ_{22}$ represent the *self*-exchange coefficients, that are accessible from MD simulations of self-diffusivities for the constituent unary systems, and determined from eq **Error! Reference source not found.**.[1] Equation **Error! Reference source not found.** is essentially an adaptation of the interpolation formula for estimation of the M-S diffusivity for binary *fluid* mixtures.[16]

The Maxwell-Stefan formulation allows the estimation of the self-diffusivities of species 1 and 2 by generalization of eq **Error! Reference source not found.** in the following manner

$$\frac{1}{D_{1,self}} = \frac{1}{Đ_1} + \frac{x_1}{Đ_{11}} + \frac{x_2}{Đ_{12}}$$

$$\frac{1}{D_{2,\text{self}}} = \frac{1}{Đ_2} + \frac{x_2}{Đ_{22}} + \frac{x_1}{Đ_{21}} \tag{8}$$

The detailed derivation of eq **Error! Reference source not found.** is provided in earlier publications.[5-7]

A step-by-step procedure for estimation of the self-diffusivities of 1 and 2 in binary mixtures is as follows.

Step 1. Determine the unary M-S diffusivities $Đ_1$ and $Đ_2$, along with the unary self-diffusivities, $D_{1,\text{self}}$ and $D_{2,\text{self}}$ using eqs **Error! Reference source not found.** and (1)

Step 2. Determine the self-exchange coefficients $Đ_{11}$ and $Đ_{22}$ using eq **Error! Reference source not found.**

Step 3. Determine the binary exchange coefficients $Đ_{12}$ using eq **Error! Reference source not found.**

Step 4. Estimate the self-diffusivities for binary mixtures $D_{1,\text{self}}$ and $D_{2,\text{self}}$ using eq **Error! Reference source not found.**

Nomenclature

Latin alphabet

$Đ_i$ Maxwell-Stefan diffusivity for molecule-wall interaction, $m^2\ s^{-1}$

$Đ_{ij}$ M-S exchange coefficient, $m^2\ s^{-1}$

$Đ_{ii}$ M-S self-exchange coefficient, $m^2\ s^{-1}$

$D_{i,self}$ self-diffusivity of species *i*, $m^2\ s^{-1}$

N number of species in the mixture, dimensionless

n_i number of molecules of species *i* in simulation box, dimensionless

N_i molar flux of species *i* with respect to framework, mol $m^{-2}\ s^{-1}$

q_i component molar loading of species *i*, mol kg^{-1}

q_t total molar loading in mixture, mol kg^{-1}

$\mathbf{r}_{l,i}(t)$ position vector for molecule *l* of species *i* at any time *t*, m

R gas constant, 8.314 J $mol^{-1}\ K^{-1}$

T absolute temperature, K

x_i mole fraction of species *i* in adsorbed phase, dimensionless

z distance coordinate, m

Greek alphabet

μ_i molar chemical potential of component *i*, J mol^{-1}

ρ framework density, kg m^{-3}

Subscripts

1 referring to component 1

2 referring to component 2

i	referring to component *i*
t	referring to total mixture

References

1. Krishna R, van Baten JM. Maxwell-Stefan modeling of slowing-down effects in mixed gas permeation across porous membranes. *J. Membr. Sci.* 2011; 383: 289-300.

2. Krishna R. Using the Maxwell-Stefan formulation for Highlighting the Influence of Interspecies (1-2) Friction on Binary Mixture Permeation across Microporous and Polymeric Membranes. *J. Membr. Sci.* 2017; 540: 261-276.

3. Krishna R. Highlighting the Influence of Thermodynamic Coupling on Kinetic Separations with Microporous Crystalline Materials. *ACS Omega.* 2019; 4: 3409-3419.

4. Krishna R. The Maxwell-Stefan Description of Mixture Diffusion in Nanoporous Crystalline Materials. *Microporous Mesoporous Mater.* 2014; 185: 30-50.

5. Krishna R. Describing the Diffusion of Guest Molecules inside Porous Structures. *J. Phys. Chem. C.* 2009; 113: 19756-19781.

6. Krishna R. Diffusion in Porous Crystalline Materials. *Chem. Soc. Rev.* 2012; 41: 3099-3118.

7. Krishna R. Occupancy Dependency of Maxwell−Stefan Diffusivities in Ordered Crystalline Microporous Materials. *ACS Omega.* 2018; 3: 15743-15753.

8. Kärger J, Ruthven DM. Diffusion in nanoporous materials: fundamental principles, insights and challenges. *New. J. Chem.* 2016; 40: 4027-4048.

9. Krishna R. Thermodynamically Consistent Methodology for Estimation of Diffusivities of Mixtures of Guest Molecules in Microporous Materials. *ACS Omega.* 2019; 4: 13520-13529.

10. Skoulidas AI, Sholl DS, Krishna R. Correlation effects in diffusion of CH_4/CF_4 mixtures in MFI zeolite. A study linking MD simulations with the Maxwell-Stefan formulation. *Langmuir*. 2003; 19: 7977-7988.

11. Krishna R. Thermodynamic Insights into the Characteristics of Unary and Mixture Permeances in Microporous Membranes. *ACS Omega*. 2019; 4: 9512-9521.

12. Krishna R, van Baten JM. Diffusion of alkane mixtures in zeolites. Validating the Maxwell-Stefan formulation using MD simulations. *J. Phys. Chem. B.* 2005; 109: 6386-6396.

13. Krishna R, van Baten JM. Investigating the potential of MgMOF-74 membranes for CO_2 capture. *J. Membr. Sci.* 2011; 377: 249-260.

14. Krishna R. The Maxwell-Stefan Description of Mixture Permeation across Nanoporous Graphene Membranes. *Chem. Eng. Res. Des.* 2018; 133: 316-325.

15. Krishna R, van Baten JM. Unified Maxwell-Stefan Description of Binary Mixture Diffusion in Micro- and Meso- Porous Materials. *Chem. Eng. Sci.* 2009; 64: 3159-3178.

16. Krishna R. Diffusing Uphill with James Clerk Maxwell and Josef Stefan. *Chem. Eng. Sci.* 2019; 195: 851-880.